Thermophysical Properties of Polyalphaolefin Oil Modified with Nanoadditives

María J.G. Guimarey[a], María J.P. Comuñas[a,*], Enriqueta R. López[a], Alfredo Amigo[b], Josefa Fernández[a]

[a] Laboratory of Thermophysical Properties, Nafomat Group, Department of Applied Physics, Faculty of Physics, University of Santiago de Compostela, 15782, Santiago de Compostela, Spain

[b] Laboratory of Thermophysical and Surface Properties of Liquids, Department of Applied Physics, Faculty of Physics, University of Santiago de Compostela, 15782, Santiago de Compostela, Spain

[*] Corresponding author. Tel.: +34 881814046; fax: +34 881814112

E-mail address: mariajp.comunas@usc.es

ABSTRACT

This article presents an experimental investigation on the effects of concentration and morphology of nanoadditives on the thermophysical properties of nanolubricants (NLs) at different temperatures. A polyalphaolefin (PAO6) oil was used as base fluid. A two-step method was used to prepare the NLs. Zirconium oxide (ZrO_2) and boron nitride (BN) nanoparticles (NPs) and graphene nanoplatelets (GnP) were separately dispersed in the base fluid with mass fraction ranging from 0.05 wt% to 2 wt%. The NPs and GnP were characterized by X-ray diffraction, Raman spectroscopy and electron microscopy. The base oil was also analyzed by mass spectrometry. Visual sedimentation, temporal variation of refractive index and Fourier transform infrared spectroscopy were used to analyze the stability of the nanolubricants and the existence of new interactions between nanoparticles and base oils. Detailed study was carried out to analyze the effect of nanoadditives on viscosity, density and adiabatic bulk modulus. Moreover, different predictive equations to estimate termophysical properties were tested using the experimental values. Pressure-viscosity coefficients as a function of the temperature and nanoparticle concentration were predicted for all the nanolubricants.

Keywords: Lubricant, ZrO_2 and Boron Nitride Nanoparticles, Graphene Nanoplatelets, Thermophysical properties.

1. INTRODUCTION

The need for energy saving is leading to the growing study of nanoaditives to be used in heat transferring [1] and lubricating [2,3] processes. Lubrication is critical to the cost effective operation and reliability of machinery. An inappropriately selected lubricant may lead to a considerable increase in the operating costs of the machine. Shahnazar et al. [4] have recently published a review that collects previous results, showing that nanoadditives can improve the performance of traditional solid lubricant additives [5-7]. However, prior to use nanolubricants (NLs), considerable knowledge about their thermophysical, tribological and rheological properties is required.

This work is part of a larger research project which has as final objective to analyze the effect of nanoadditives concentration, morphology, temperature and pressure on the nanolubricant properties. The results presented here are a first study on how nanoadditives affect thermophysical properties of polyalphaolefins (PAOs). These base oils are full synthetic and are classified on the group IV of the categorization reported by the American Petroleum Institute. PAOs are the most commonly used synthetic base fluids in lubricant formulation. The physical and chemical properties of PAOs make them attractive for a variety of applications requiring a wider temperature operating range than that normally covered by mineral oils [8]. PAOs are saturated hydrocarbons of well-defined molecular weight. They are manufactured by a two-steps process from linear alphaolefins, generally 1-decene. An advantage of PAOs is that they can be tailor-made to fit the requirements of the end-use application [9]. This can be done by manipulating the reaction variables, such as chain length of olefin feedstock, temperature, time, catalyst type and concentration, and distillation.

PAOs are usually named by their kinematic viscosity at T = 373.15 K in $mm^2 \cdot s^{-1}$. In this work we have focused our attention on PAO6, that means a kinematic viscosity around 6 $mm^2 \cdot s^{-1}$ at T = 373.15 K. PAO6 is used as industrial bearing oils, hydraulic oils, aviation

lubricants, drilling fluids, heat transfer fluids, dielectric fluids and greases [10]. As additives we used ZrO_2 nanoparticles, boron nitride (BN) nanoparticles and graphene nanoplatelets (GnP). The first nanoparticles were chosen to complete our previous work [11] concerning nanolubricants based on other synthetic oils (polyalkyleneglycol (PAG2), biodegradable polymeric ester (BIOE) and isotridecyl trimellitate (TTM)) and ZrO_2 nanoparticles at mass concentration up to 2 wt%. The other two nanoadditives (BN and GnP) were studied with the aim to improve the stability of the nanolubricants based on PAO6 and ZrO_2.

In recent years several studies were published about nanolubricants based on polyalphaolefins, mainly on tribological and antiwear properties. Thus, Nunn et al. [12] have compared the friction coefficient and wear of a PAO oil containing nanodiamond particles, onion-like carbon, single/multiwall carbon nanotubes or graphene nanoplatelets. Hernández Battez et al. [13] studied the tribological behavior of nanolubricants based on PAO6 and ZnO nanoparticles. They also use two esters as dispersing agents (OL100 and OL300). These authors conclude that ZnO nanoadditives reduce wear at extreme pressure conditions. Hernández Battez et al. [14-16] have also analyzed the effect of other nanoparticles such as CuO and ZrO_2 dispersed in PAO6 at 0.5% to 2% nanoparticle mass concentration. Viesca et al. [17] study the influence of the addition of carbon-coated copper nanoparticles on the tribological behavior of PAO6 and compare it with the case of non-coated copper nanoparticles. Zhang et al. [18] and Chou et al. [19] use the same base oil together with Nickel nanoparticles as additives showing a decrease of the average friction coefficient and wear. Nesappan et al. [20] have evaluated the tribological characteristics of nanolubricants based on polyalphaolefins aditivated with Cu or CuO for their use in machine tool slideways. Demas et al. [21] have studied the friction and wear of another polyalphaolefin (PAO10) base oil additivated with 3 wt% of BN or of molybdenum disulfide (MoS_2) nanoparticles. Shahmohamadi et al. [22] analyze the tribological performance of carbon nanoparticles dispersed in PAO6. The above studies and many other similar investigations have shown the

advantages of using nanoparticles in reducing friction. However, there are still few studies and reviews focusing particularly on the effects of nanoparticle shape, size, concentration and Brownian motion on the thermophysical properties, mainly flow properties (viscosity), of nanolubricants. This analysis is also of major importance for the final implementation of the nanolubricants in the industry.

2. EXPERIMENTAL SECTION

2.1. Materials: characterization

Table 1 shows the source and mole fraction purity of the samples used in this work. The base oil (PAO6) has been kindly provided by Repsol. ~~A schematic representation of the typical linear tetramer of this fluid is presented in Figure 1.~~ PAO6 is an oligomer composed by molecules of different number and size of alkyl chains (trimers, tetramers and pentamers among others). From the NMR and gas-chromatography analysis performed by the supplier it can be concluded that the most representative component in the chemical composition of our sample is a tetramer. Moreover, the NMR indicates that the sample have around 57% of linear chains and 43% of branched ones. MALDI-TOF [23] mass spectrometry by means of Ultraflex III Tof/Tof (Bruker) equipment has been used for the characterization of this fluid. This oil presents a weight-average molecular weight, M_w, of 604.3 $g \cdot mol^{-1}$ and a polydispersity index of M_w/M_n=1.043. A schematic representation of a typical linear tetramer of PAO6 is presented in Figure 1.

The nanoadditives were supplied by Iolitec. Thus, ZrO_2 nanoparticles have a purity of 99.9% (lot INO059008), a nominal diameter of 30-60 nm and a bulk density of 5.9 $g \cdot cm^{-3}$. Boron nitride (BN) nanoparticles present a purity of 99% (lot MNC018001,) a nominal diameter of 70 nm and a bulk density of 2.29 $g.cm^{-3}$. Graphene nanoplatelets shows a purity of 99.5% (lot NCP068011), a medium size of 11-15 nm and a bulk density of 2.25 $g.cm^{-3}$. ZrO_2 and BN nanopowders were characterized by X-ray diffraction (XRD) using a Philips

type powder diffractometer (Cu Kα1 irradiation, λ(Kα1)=1.5406Å), with an accelerating voltage of 40 kV and an applied current of 30 mA. The X-ray patterns of ZrO_2 nanopowder present sharp and well defined peaks. Figure 2a shows a high degree of crystallinity which corresponds to monoclinic ZrO_2 crystal phase, as explained in our previous work [11]. The X-ray patterns of BN nanopowder is shown in Figure 2b. The main peak at 26.27° corresponds to the characteristic (002) reflection and another broad peak in the range of 40–45° covering the unresolved reflections (100) and (101). It can be seen that all diffraction peaks agree well with standard data for the bulk BN with a layered hexagonal structure [24]. Hexagonal boron nitride has the following lattice parameters: a = 0.2504 nm, b = 0.2504 nm; c = 0.6661 nm, according with literature data [25]. The measured interlayer distance of the (002) planes is larger than ~0.33 nm, which is typical to well-crystalline BN [26].

Graphene nanoplatelets were characterized by Raman spectroscopy in the visible range, exactly at a wavelength of 514 nm, to identify the number of graphene layers. As it is shown in the Figure 3, graphene nanosheets correspond to a multilayer type due to the high intensity (at 1581 cm^{-1}) and the pronounced width of the G-band. The G´ band appears at 2726 cm^{-1} and the D-band at about half of the frequency of the G´ band at 1357 cm^{-1} [27].

The morphology, size and spectrum composition of three nanoparticles were obtained by scanning electron microscopy (SEM, Zeiss FESEM Ultra Plus) equipped with an additional detector for energy dispersive X-ray microanalysis (EDX). We could observe in Figure 4 that ZrO_2 nanoparticles are spherical, BN powder shows a rod-like morphology [28], and the graphene nanoplatelets a laminar structure. In relation to elemental microanalysis (Figure 5), for ZrO_2 nanoparticles the results indicate the predominant presence of zirconium and oxygen in the sample. The content of hafnium is due to the manufacturer uses 3% HfO_2 to stabilize the ZrO_2 nanoparticles. In the case of BN nanopowders, EDX confirms that the purity is approximately 99% and shows a composition of 36.40% atomic boron and 47.7% atomic nitrogen which demonstrates the stoichiometry

between B:N is approximately 1:1. EDX analysis of graphene nanoplatelets show the presence of oxygen impurities probably from the synthetic route of GnP. Another reason could be that its large specific surface area can easily adsorb great amounts of oxygen molecules on the surface [29]. The aggregation state of the nanoparticles in n-butanol was evaluated trough transmission electron microscopy (TEM, JEOL JEM-2010) by using an accelerating voltage of 200 kV. Figure 6 reveals nanoadditives agglomeration mainly due to the high surface area and surface activity of the nanoparticles [30].

2.2. Nanolubricant Preparation

Two-step method was used to prepare the nanolubricants. Firstly, we mixed the nanoadditives (ZrO_2, BN or GnP) in form of dry powder, with the base oil (PAO6). A high precision balance Sartorius MC 210P was used to determine the mass concentration of nanoparticles. The readability of the balance in the measured mass range is 0.00001 g. Secondly, we disperse the nanoparticles in the base oil (approximately 20 ml) by using an ultrasonic method. To prepare the nanolubricants containing ZrO_2 or BN a disruptor (HD 2200 Sonopuls) was used. The sonicator probe conducts the acoustic energy from the transducer into the sample. The factors that affect the energy transferred to the nanodispersion were detailed in our previous article [11]. In this work, we have used the probe MS73 which has a diameter of 3 mm, a power of 200 W, an amplitude of 302 μm and a sonication time of 30 minutes. To minimize overheating during sonication, the dispersions were immersed in an ice-water bath. To prepare the nanolubricants containing graphene nanoplatelets a Fisherbrand ultrasonic bath, with continuous shaking periods of 2 hours and at a shaking frequency of 37 kHz, was used. We have prepared nine nanolubricants (three for each additive) with different mass concentrations. For ZrO_2 nanoparticles we have selected mass concentrations (0.5 wt%, 1 wt% and 2 wt%) similar to those used in our previous work [11] with the aim to compare the behavior of these nanolubricants (PAO6 +

ZrO_2) with those formulated from other base oils (polyalkyleneglycol + ZrO_2, biodegradable polymeric ester + ZrO_2 and isotridecyl trimellitate + ZrO_2). For BN and GnP we have chosen as mass concentration 0.05 wt%, 0.10 wt% and 0.25 wt% with the aim to improve the stability reducing the mass concentration of nanoadditives.

Fourier transform infrared spectrometry (FTIR, VARIAN 670-IR) analyses were conducted to study the formation of chemical bonds between nanoparticles and the base oil. Figure 7 shows two intense bands at 2852 and 2920 cm^{-1} for the base oil (PAO6) that correspond to C-H stretching vibrations of the aliphatic carbon chain and two medium intensity bands at wavenumbers of 1377 and 1463 cm^{-1} that can be attributed to the C-H deformation of the aliphatic group $–CH_3$ [31]. Figure 7 also shows that the IR absorbance spectra of the nanolubricants are similar to that of the base oil. No new spectral peaks or shifts are found for the dispersions in comparison with the base oil, which indicates that no chemical bonds were formed.

Visual observation is the simplest method to initially evaluate stability of nanolubricants. In this work, the nanolubricants were kept at room temperature without any disturbance. Subsequently, the samples were observed every hour until detecting the nanoparticles sedimentation at the bottom of the container. Figure 8 shows photographs displaying the temporal evolution of the nanolubricants. As can be seen in this figure, nanolubricants additivated with ZrO_2 present the poorest stability. Thus, a practically complete sedimentation occurs after 24 hours. It is interesting to remark that the sedimentation we found for nanolubricants based on PAO6 and ZrO_2 is faster than those observed in our previous work [11] when other base oils (PAG2, BIOE and TTM) were used with the same nanoparticles (ZrO_2) and the same mass concentration (2 wt%). Furthermore, we have measured the temporal evolution of the refractive index of the nanolubricants in order to determine how useful is this tool to qualitative quantify the stability of nanolubricants. This method was presented in a previous work [11]. Thus, a refractometer

(Mettler Toledo RA-510M) which operates at the wavelength of the D-line of sodium (589.3 nm) was used to register the temporal evolution of the refractive index (n) at T = 298.15 K. Figure 9 shows the variation of the refractive index over a time interval of 45 hours. The overall variation of the refractive index during the 6 first hours after sonication is 0.02 when PAO6 is used as base oil and ZrO_2 nanopowder as nanoadditive, whereas the variation was 0.002 for PAG2 and 0.001 for TTM based nanolubricants [11]. These results are in agreement with the Stokes's law, due to sedimentation velocity is inversely proportional to viscosity of the fluid through which solid particles precipitate [32]. Thus, dynamic viscosity at T = 293.15 K of PAO6 is around 58 mPa·s, whereas for PAG2, TTM and BIOE the values are 143 mPa·s, 1449 mPa·s and 1652 mPa·s, respectively.

For nanolubricants containing PAO6 as base oil the stability seems to be improved when GnP nanoadditives are used instead of ZrO_2 and the mass concentration is reduced. Thus, sedimentation seems to be slower for the nanolubricants additivated with graphene nanoplatelets. The overall variation of the refractive index during the first six hours after sonication is 0.0004 for PAO 6 + 0.25 wt% BN and 0.0002 for PAO6 + 0.25 wt% GnP nanolubricants. Another interesting observation is that despite the fact that stability of ZrO_2 nanolubricants seems to be poorest, sedimentation does not significantly affect the thermophysical property measurements. In this sense, no fluctuation of density, viscosity and speed of sound was observed during the time interval (2 hours) required to perform each experiment.

2.3. Measurements technique

Density at atmospheric pressure of the nanolubricants was measured from (278.15 to 373.15) K by using a vibrating densimeter Anton Paar SVM 3000 Stabinger. The temperature of the cell is controlled through an integrated thermostat with cascaded Peltier elements and measured with a Pt100 thermometer with an expanded (k=2) uncertainty of 0.02 K. Density

cell consists in a glass U-tube, which is excited to produce mechanical resonant vibrations according to DIN 51757 standard. The expanded (k=2) uncertainty of density measurements performed with SVM 3000 Stabinger is 0.0005 g·cm^{-3}. Density values obtained directly from mechanical oscillator densimeters do not often include the effect that the sample viscosity has on the measurement. In such cases, it is necessary to apply a correction factor. Anton Paar SVM 3000 Stabinger reports directly the corrected density value. To check the consistency of the measurements, which is important in the case of nanolubricants based on ZrO_2 nanoparticles due to their faster sedimentation, density of nanolubricants has also been measured with another vibrating tube densimeter (Anton Paar DSA 5000) that can work at 0.1 MPa from (283.15 to 338.15) K. The upper limit for the standard uncertainty of density measurements (samples with viscosity higher than 100 mPa·s) performed with DSA 5000 is 0.0002 g·cm^{-3}. For samples with a viscosity lower than 30 mPa·s, a standard uncertainty of 0.00004 g·cm^{-3} is obtained. The speed of sound was also measured (at an operating frequency of approximately 3 MHz) by using this device from (283.15 to 338.15) K, with a standard uncertainty of 2 m·s^{-1}. Viscosity at atmospheric pressure was also measured with the Anton Paar Stabinger SVM 3000 rotational viscometer. This apparatus allows measuring dynamic and kinematic viscosities from (278.15 to 373.15) K, in a viscosity range from 0.2 mPa·s to 20 Pa·s. The SVM 3000 Stabinger viscometer has a cylindrical geometry and it is based on a modified Couette principle with a rapidly rotating outer tube and an inner measuring bob that rotates more slowly. Relative expanded (k=2) uncertainty of 1% has been estimated for the dynamic viscosity.

3. RESULTS AND DISCUSSION

Densities obtained for the base oil (PAO6) with SVM 3000 Stabinger and DSA 5000 densimeters are reported in Table 2. The average absolute deviation (*AAD%*) between the values obtained for PAO6 with both apparatuses is 0.03%. Density values obtained with

SVM 3000 Stabinger and DSA 5000 for the nine nanolubricants are reported in Tables 3 and 4, respectively. As can be seen in Figure 10 nanolubricants density data determined with SVM 3000 Stabinger are also in agreement with those provided by Anton Paar DSA 5000. Thus, *AADs* of 0.05%, 0.10%, and 0.07% were found for PAO6/ZrO_2 at 0.5 wt%, 1 wt% and 2 wt%, respectively. Similarly, *AAD* values are 0.03%, 0.03% and 0.07% for PAO6/BN and 0.04%, 0.03% and 0.04% for PAO6/GnP dispersions for 0.05 wt%, 0.1 wt% and 0.25 wt% respectively. These deviations confirm the good agreement between the measurements performed with both apparatuses (SVM 3000 Stabinger and DSA 5000) for the nine nanolubricants. For all nanolubricants, density increases with the mass concentration of nanoparticles. Data reveal that studied ZrO_2 nanofluids at 0.5 wt%, 1 wt% and 2 wt% produces an increase on the density of PAO6 around 0.5%, 1.0% and 1.9%, respectively. In previous work [11] we have found that the additivation of other synthetic base oils (PAG2, BIOE and TTM) with a 2 wt% of ZrO_2 produced an increase of the density around 1.8%. So the influence of the addition of ZrO_2 is quite similar for the four base oils (Figure 11a). If we focus our attention in PAO6 base oil, we can observe that the addition of BN and GnP at 0.25 wt% implies an increase of 0.3% in density respect to that of this base oil. This increase is half of that obtained with ZrO_2 for twice mass concentration. Thus, we can conclude (Figure 11b) that the shape, chemical structure or morphology of nanoparticles (spherical for ZrO_2, rod-like for BN and laminar for GnP) seem to have no significant effect on density values of these nanolubricants. The mass concentration of nanoadditives has influence on the final density of the nanolubricant. Thus, increases up to 2% were found for the nanolubricants studied in this work.

The values of the speed of sound of the neat base oil and the nine nanolubricants from (283.15 to 338.15) K are reported in Table 5. For PAO6 base oil, a value of 1466 $m \cdot s^{-1}$ at T = 283.15 K was obtained. This value is slightly higher than that previous found [11] for PAG2 (1382 $m \cdot s^{-1}$) and lower than those of TTM (1508 $m \cdot s^{-1}$) and of BIOE (1523 $m \cdot s^{-1}$

[1]). In this table it can be appreciated that speed of sound of all nanolubricants decreases with the rise of temperature following the common behavior of non-aqueous liquids. Several acoustic parameters, such as adiabatic compressibility coefficient (β) can been determined from the experimental density and speed of sound data. In this work, the β parameter or its inverse, the adiabatic bulk modulus (K_S) of the nanolubricants was determined using the Newton-Laplace´s relation:

$$\beta = 1/\rho u^2 = 1/K_S \tag{1}$$

In figure 12 the adiabatic bulk modulus was plotted as a function of density over all the temperature interval. The dependence of the adiabatic bulk modulus on nanoparticles concentration is negligible at low mass concentrations (from 0.05 to 0.25 wt%). This is the case of the PAO6/BN and PAO6/GnP nanolubricants for which the values we found are similar to those of the base oil (PAO6). Data reveal that studied ZrO_2 nanolubricants at 0.5 wt%, 1 wt% and 2 wt% produce increases on the adiabatic bulk modulus of PAO6 around 0.3%, 1.1% and 0.8%, respectively. As in previous work [11], where other synthetic base oils were studied, we have not observed a regular dependence of this property with the ZrO_2 nanoparticle mass concentration.

The bulk modulus of lubricating oils is a predominant factor affecting traction behavior in high-pressure elastohydrodynamic contacts [33]. The use of the adiabatic bulk modulus as predictive parameter for pressure-viscosity coefficient (α) of oils was previous investigated [34]. This coefficient is an important parameter to characterize the suitability of a lubricant for elastohydrodynamic lubrication regime. Usually, the equation employed to calculate the local pressure-viscosity coefficient is as follows:

$$\alpha(p) = \frac{1}{\eta(p,T)}\left(\frac{\partial \eta(p,T)}{\partial p}\right)_T \tag{2}$$

Thus to evaluate α it is necessary to know the viscous behavior for the lubricants under study as a function of both the temperature and the pressure. When the pressure dependence of the viscosity is not available, Mia and Ohno [35] have proposed a method to predict the pressure-viscosity coefficient from the adiabatic bulk modulus. These authors report different expressions depending on the base oil. For polyalphaolefins they find:

$$\alpha = 2.03 \exp\left(1.16 K_s\right) \tag{3}$$

Using the above equation, we have obtained an α value of 11.6 GPa^{-1} at T = 313.15 K at 0.1 MPa for the PAO6 base oil. This value is in agreement with data previously published by Lafont et al. [36] (11.5 GPa^{-1} at the same temperature). In Figure 13a we have also plotted the pressure-viscosity coefficient for the base oil (PAO6) together with those for other polyalphaolefins [37] and mineral and synthetic oils [38] at T = 313.15 K. As can be observed in this figure the α-coefficient obtained from equation (3) for PAO6 is lower than those of PAO32 and PAO40. Thus, this coefficient seems to increase with the branching degree of the polyalphaolefins. Similar fact has been previously observed for esters [39] and polyolester [40] lubricants. We observe also that α values for polyalphaolefins are lower than those previously obtained for mineral oils [38]. Subsequently, equation (3) has also been used to estimate the pressure-viscosity coefficient of the nine nanolubricants. As expected from the behaviour of the bulk modulus with the concentration (Figure 13b), the α-coefficient obtained from equation (3) varies smoothly with the nanoparticles morphology and concentration. Mia and Ohno have also observed that lubricating oils with low values of adiabatic bulk modulus present good low temperature fluidity. From these results, we can conclude that the nine nanolubricants would have similar low temperature fluidity independently of the nanoadditive.

Base oil and nanolubricants viscosities measured by SVM 3000 densimeter as a function of nanoadditive concentration in the temperature range from (278.15 K to 373.15)

K are given in Table 6. Dynamic viscosity behavior has been described using the following expression:

$$\eta(T) = A\exp\left(\frac{B}{T-C}\right) \tag{4}$$

The parameter values (*A*, *B* and *C*) we found for each nanolubricant are reported in Table 7. This equation reproduces the experimental values reported in Table 6 with average relative deviations around 0.5% for nanolubricants additivated with ZrO_2 and BN and 0.4% with GnP. With the addition of ZrO_2 nanoparticles, the viscosity of PAO6 increases up to 1.3%, 2.4% and 6.6% over the temperature range for mass concentrations of 0.5, 1 and 2 wt%, respectively. In Figure 14a the increase of viscosity with respect to the base oil over all the temperature range was plotted for PAO6 additivated with 2.0 wt% of ZrO_2. In this figure we present also the results previously obtained [11] for PAG2/2wt% (an increase of 3.9%), TTM/2wt% (an increase of 6.5%) and BIOE/2wt% (an increase of 3.9%) nanolubricants. So, increases around 4% are found for PAG2 and BIOE whereas they are around 7% for PAO6 and TTM base oils.

As can be seen in Figure 14b the increase in the viscosity of the base oil (PAO6) due to the addition of BN nanoparticles is around 0.6% and 1.9% over all the temperature interval for the concentrations of 0.05 and 0.25 wt%, respectively. The increase observed for GnP at 0.25 wt% concentration is 4.8%. We can conclude that the morphology and concentration of the nanoadditives have more effect on the viscosity (Figure 14b) than on the density (Figure 11b) of nanolubricants. If the viscosity of the final nanolubricant increases due to the presence of nanoadditives, a higher pressure drop in the tubes can occur and subsequently an increase in the power consumption of the machine. The dependence of the relative dynamic viscosity with the nanoadditives volume fraction at T = 298.15 K has been plotted in Figure 15 for all the nanolubricants studied in the present work together with those values obtained previously for TTM/ZrO_2, PAG2/ZrO_2 and BIOE/ZrO_2 nanolubricants. As can be

seen the greatest increase in viscosity is obtained when GnP is used as additive. This fact may be due to its flat morphology. Thus, spherical (ZrO_2) and rod-like structures (BN) could be placed among the layers of the oil as others authors have remarked [41]. This effect could not occur in the case of GnP due to its laminar shape and subsequently the viscosity increases more quickly. Viscosity index (*VI*) has also been determined by using SVM Stabinger device. This equipment has a built-in function to determine the viscosity index according to ASTM D2270 standard. This property does not present a regular dependence with the nanoparticle mass concentration as shows Figure 16. Thus, a linear dependence of *VI* with the mass concentration was only obtained for the nanolubricants formulated with BN nanoadditives. This is not the case for the nanolubricants containing ZrO_2 and GnP. Moreover, PAO6/2wt%ZrO_2 has similar *VI* than PAO6/0.10wt%GnP.

Densities reported in Table 3 for the nine nanolubricants were also compared with those predicted by the models collected on Table 8. Figure 17 shows relative density deviations between experimental density data and the values predicted by Wasp et al. [42] and Pak and Cho [43] models. *AAD%* obtained for all nanolubricants have been lower or equal than 0.15% and 0.17% with Pak and Cho and Wasp et al. equations, respectively. For both models the highest relative deviations corresponds to 1.0 wt% ZrO_2 nanodispersion. These results are similar to those previously found [11] for nanolubricants containing ZrO_2 nanoparticles and (polyalkyleneglycol, biodegradable polymeric ester and isotridecyl trimellitate) base oils. Moreover, for the most of the temperature interval and mass concentrations both models under predict the density values.

There is a great variety of models proposed to predict the viscosity of nanofluids taking into account different factors [44]. We have applied the viscosity models reported in Table 8, which are the most frequently used. The absolute average relative deviations between the viscosities obtained with the predictive models and the experimental data are plotted in Figure 18. For each nanolubricant (PAO6/ZrO_2, PAO6/BN and PAO6/GnP) the

deviations increase with the increment of the nanoadditive mass concentration. The highest deviations are obtained with Einstein [45], Saito [46], Brinkman [47] and Batchelor [48] models. Moreover, these four models predict very similar viscosityvalues for all the nanolubricants studied in this work. The best results are always found with the Chen et al. [49] model followed by Whang et al. [50] equation for which relative deviations around 3.2%, 0.9% and 3.7% are found for PAO6/2wt%ZrO_2, PAO6/0.25wt%BN and PAO6/0.25wt%GnP, respectively. Other authors [51] have previously found good results with the Chen et al., which is a modification of the Krieger-Dougherty equation by considering the effects of packing fraction within the aggregate structure of additives [35]. Due to the additives form aggregates inside the base oil (PAO6) we should expect that this model provides the lower deviations with the experimental densities. For the nanolubricant based on PAO6 additivated with ZrO_2, the deviations obtained with all the models are quite similar to those previously found [11] for TTM/ZrO_2 nanolubricant, and higher than those observed for PAG2/ZrO_2 and BIOE/ZrO_2 nanolubricants. This tendency was also reported above for the increase in viscosity due to the presence of nanoadditives (viscosity increases around 4% for PAG2 and BIOE whereas around 7% for PAO6 and TTM based nanolubricants). It is also interesting to note that the relative deviations are much higher for GnP additives than for BN nanoparticles even if the same mass concentration is used. Likewise, relative deviations when GnP nanosheets are used at 0.25 wt% mass concentration are closer to those found for ZrO_2 at 2 wt%. This fact could be due to most of the models are based on the assumption of viscous fluid containing spherical particles, and the flat morphology of GnP is far to this assumption. The theoretical models indicated in Table 8 do not take into account the different geometries of the nanoparticles. Ghozatloo et al. [52] have proposed a correction that takes into account a morphology factor. These authors report the value of this factor for spherical, cylindrical and sheet geometries. We have tried to use this

correction but the results found are practically the same than those obtained without taking into this correction.

4. CONCLUSIONS

Detailed experimental investigation on effects of concentration and morphology of nanoadditives on some thermophysical properties of nanolubricants based on PAO6 and zirconium oxide, boron nitride or graphene nanoplatelets at mass concentration from 0.05 wt% to 2 wt% was carried out. The main findings of this work are:

- The sedimentation of ZrO_2 nanoparticles is faster in PAO6 than in polyalkyleneglycol, polymeric ester or isotridecyl trimellitate base oils.
- GnP nanoadditives lead to PAO6 based nanolubricants with slightly better stability.
- The shorter stability of the PAO6 based nanolubricants does not affect thermophysical property measurements. Thus, no fluctuations were observed during the experiments.
- The morphology and concentration of the ZrO_2, BN and GnP nanoadditives have stronger effect on the viscosity than on the density of PAO6 based nanolubricants.
- The dispersion of nanoadditives with laminar shape provokes a larger increase on the viscosity of the polyalphaolefin base oil than those with spherical or rod-like morphologies.
- Viscosity indexes of PAO6/ZrO_2, PAO6/BN and PAO6/GnP nanolubricants have not a regular dependence with the mass concentration of nanoadditives.
- Models considering the effects of packing fraction within the aggregate structure of additives predict better the viscosity of PAO6 based nanolubricants.

Nomenclature

M_w	Weight average molecular mass ($g \cdot mol^{-1}$)
M_n	Number average molecular mass ($g \cdot mol^{-1}$)
n	Refractive index
T	Temperature (K)
p	Pressure (Pa)
ρ	Density ($g \cdot cm^{-3}$)
u	Speed of sound ($m \cdot s^{-1}$)
K_s	Adiabatic bulk modulus (GPa)
β	Adiabatic compressibility (GPa^{-1})
α	Pressure-viscosity coefficient
η	Viscosity (Pa·s)
ϕ	Particle volume fraction
φ	Particle mass fraction
AAD	Average absolute deviations

SUBSCRIPTS

exp	Experimental value
np	Nanoparticle
bf	Base fluid
nf	Nanofluid
pre	Predicted value

Notes. Authors declare no competing financial interest.

ACKNOWLEDGMENTS

Authors acknowledge REPSOL for the PAO6 sample. This work was supported by both the Spanish Ministry of Economy and Competitiveness and the UE FEDER programme through ENE2014-55489-C2-1-R and ENE2017-86425-C2-2-R projects. Moreover, this work was funded by the Xunta de Galicia and UE FEDER (GRC ED431C 2016/001). Authors would like to thank the use of RIAIDT-USC analytical facilities.

REFERENCES

[1] J.M. Munyalo, X. Zhang, Particle size effect on thermophysical properties of nanofluid and nanofluid based phase change materials: A review, J. Mol. Liquids 265 (2018) 77-87.

[2] M. Hemmat Esfe, H. Rostamian, M. Reza Sarlak, A novel study on rheological behavior of ZnO-MWCNT/10w40 nanofluid for automotive engines, J. Mol. Liquids 254 (2018) 406-413.

[3] S.S. Sanukrishna, S. Vishnu, M. Jose Prakash, Experimental investigation on thermal and rheological behaviour of PAG lubricant modified with SiO_2 nanoparticles, J. Mol. Liquids 261 (2018) 411-422.

[4] S. Shahnazar, S. Bagheri, S.B. Abd Hamid, Enhancing lubricant properties by nanoparticle additives, Int. J. Hyd. Energy 41 (2016) 3153-3170.

[5] S.S.N. Azman, N.W.M. Zulkifli, H. Masjuki, M. Gulzar, R. Zahid, Study of tribological properties of lubricating oil blend added with graphene nanoplatelets, J. Mater. Res. 31 (2016) 1932-1938.

[6] Q. Wan, Y. Jin, P. Sun, Y. Ding, Tribological Behaviour of a Lubricant Oil Containing Boron Nitride Nanoparticles, Procedia Eng. 102 (2015) 1038-1045.

[7] Y. Xu, Y. Peng, K.D. Dearn, X. Zhegn, L. Yao, X. Hu, Synergistic lubricating behaviors of graphene and MoS_2 dispersed in esterified bio-oil for steel/steel contact, Wear 342-343 (2015) 297-309.

[8] L.R. Rudnick, Polyalphaolefins in: Synthetic, Mineral Oils and Bio-based Lubricants: Chemistry and Technology, Second Edition, 2013.

[9] R. Benda, J. Bullen, A. Plomer, Synthetics basics: Polyalphaolefins — base fluids for high-performance lubricants, J. Synth. Lub. 13 (1996) 41-57.

[10] Chevron Phillips Chemical Company, Safe handling and storage of Synfluids® polyalphaolefins (PAO) (2008)

[11] M.J.G. Guimarey, M.R. Salgado, M.J.P. Comuñas, E.R. López, A. Amigo, D. Cabaleiro, L. Lugo, J. Fernández, Effect of ZrO_2 nanoparticles on thermophysical and rheological properties of three synthetic oils, J. Mol. Liquids 262 (2018) 126-138.

[12] N. Nunn, Z. Mahbooba, M.G. Ivanov, D.M. Ivanov, D.W. Brenner, O. Shenderova, Tribological properties of polyalphaolefin oil modified with nanocarbon additives, Diam. Relat. Mater. 54 (2015) 97-102.

[13] A. Hernandez Battez, J.E. Fernandez Rico, A. Navas Arias, J.L. Viesca Rodriguez, R. Chou Rodriguez, J.M. Diaz Fernandez, The tribological behaviour of ZnO nanoparticles as an additive to PAO6, Wear 261 (2006) 256-263.

[14] A. Hernández Battez, R. González, D. Felgueroso, J.E. Fernández, M. del Rocío Fernández, M.A. García, I. Peñuelas, Wear prevention behaviour of nanoparticle suspension under extreme pressure conditions, Wear 263 (2007) 1568-1574.

[15] A. Hernández Battez, R. González, J.L. Viesca, J.E. Fernández, J.M. Díaz Fernández, A. Machado, R. Chou, J. Riba, CuO, ZrO_2 and ZnO nanoparticles as antiwear additive in oil lubricants, Wear 265 (2008) 422-428.

[16] A. Hernández Battez, J.L. Viesca, R. González, D. Blanco, E. Asedegbega, A. Osorio, Friction reduction properties of a CuO nanolubricant used as lubricant for a NiCrBSi coating, Wear 268 (2010) 325-328.

[17] J.L. Viesca, A. Hernández Battez, R. González, R. Chou, J.J. Cabello, Antiwear properties of carbon-coated copper nanoparticles used as an additive to a polyalphaolefin, Tribol. Int. 44 (2011) 829-833.

[18] Y. Zhang, S. Zhang, P. Zhang, G. Yang, Z. Zhang, Preparation of Nickel-Based Nanolubricants and Investigation of their Tribological Behavior, Advances in Tribology, 2016.

[19] R. Chou, A.H. Battez, J.J. Cabello, J.L. Viesca, A. Osorio, A. Sagastume, Tribological behavior of polyalphaolefin with the addition of nickel nanoparticles, Tribol. Int. 43 (2010) 2327-2332.

[20] S. Nesappan, N. Palanisamy, M. Chandarn, Tribological investigation of copper (Cu) and Copper oxide (CuO) nanoparticles based nanolubricants for machine tool slideways,

ASME International Mechanical Engineering Congress and Exposition, Proceedings (IMECE), 2014.

[21] N.G. Demas, E.V. Timofeeva, J.L. Routbort, G.R. Fenske, Tribological Effects of BN and MoS_2 Nanoparticles Added to Polyalphaolefin Oil in Piston Skirt/Cylinder Liner Tests, Tribol. Lett. 47 (2012) 91-102.

[22] H. Shahmohamadi, R. Rahmani, H. Rahnejat, C.P. Garner, N. Balodimos, Thermohydrodynamics of lubricant flow with carbon nanoparticles in tribological contacts, Tribol. Int. 113 (2017) 50-57.

[23] H.J. Räder, W. Schrepp, MALDI-TOF mass spectrometry in the analysis of synthetic polymers, Acta Polym. 49 (1998) 272-293.

[24] C. Huang, C. Chen, X. Ye, W. Ye, J. Hu, C. Xu, X. Qiu, Stable colloidal boron nitride nanosheet dispersion and its potential application in catalysis, J. Mater. Chem. A 1 (2013) 12192-12197.

[25] R.T. Paine, C.K. Narula, Synthetic routes to boron nitride, Chem. Rev. 90 (1990) 73-91.

[26] T. Chengchun, B. Yoshio, H. Yang, Z. Chunyi, G. Dmitri, Synthetic Routes and Formation Mechanisms of Spherical Boron Nitride Nanoparticles, Adv. Funct. Mater. 18 (2008) 3653-3661.

[27] A.C. Ferrari, J.C. Meyer, V. Scardaci, C. Casiraghi, M. Lazzeri, F. Mauri, S. Piscanec, D. Jiang, K.S. Novoselov, S. Roth, A.K. Geim, Raman Spectrum of Graphene and Graphene Layers, Phys. Rev. Lett. 97 (2006) 187401.

[28] R.N. Muthu, S. Rajashabala, R. Kannan, Synthesis, characterization of hexagonal boron nitride nanoparticles decorated halloysite nanoclay composite and its application as hydrogen storage medium, Renew. Energ. 90 (2016) 554-564.

[29] X. Zhang, S. Wan, J. Pu, L. Wang, X. Liu, Highly hydrophobic and adhesive performance of graphene films, J. Mater. Chem. 21 (2011) 12251-12258.

[30] W. Yu, H. Xie, A Review on Nanofluids: Preparation, Stability Mechanisms, and Applications, J. Nanomater. 2012 (2012) 17.

[31] R. González, A.H. Battez, J.L. Viesca, A. Higuera-Garrido, A. Fernández-González, Lubrication of DLC Coatings with Two Tris(pentafluoroethyl)trifluorophosphate Anion-Based Ionic Liquids, Tribol. Trans. 56 (2013) 887-895.

[32] L. Kong, J. Sun, Y. Bao, Preparation, characterization and tribological mechanism of nanofluids, RSC Advances 7 (2017) 12599-12609.

[33] N. Ohno, M.Z. Rahman, K. Kakuda, Bulk Modulus of Lubricating Oils as Predominant Factor Affecting Tractional Behavior in High-Pressure Elastohydrodynamic Contacts, Tribol. Trans. 48 (2005) 165-170.

[34] S. Mia, Prediction of Tribological and Rheological Properties of Lubricating Oils by Sound Velocity, Saga University (2010)

[35] S. Mia, N. Ohno, Relation between low temperature fluidity and sound velocity of lubricating oil, Tribol. Int. 43 (2010) 1043-1047.

[36] P. Lafont, J. Echávarri, E.D.L. Guerra, E. Chacón, A. Díaz, J.M. Muñoz-Guijosa, J.L.M. Sanz, J. Muñoz, Caracterización del comportamiento reológico de lubricantes mediante ensayo en tribómetro, XVIII Congreso Nacional de Ingeniería Mecánica Málaga, 2010.

[37] S. Mia, S. Mizukami, R. Fukuda, S. Morita, N. Ohno, High-pressure behavior and tribological properties of wind turbine gear oil, J Mech. Sci. Technol. 24 (2010) 111-114.

[38] E. Höglund, Influence of lubricant properties on elastohydrodynamic lubrication, Wear 232 (1999) 176-184.

[39] S.J. Randles, Esters, in Synthetic, Mineral Oils, and Bio-Based Lubricants: Chemistry and Technology, Taylor and Francis Ed., 2006.

[40] U.J. Jonsson, K.C. Lilje, Elastohydrodynamic Lubrication Properties of Polyol Ester Lubricants-R134a Mixtures, Proceedings of 1998 International Compressor Engineering Conference at Purdue, Purdue University USA, July 14-17, 1998, pp. 123-128.

[41] E. Ettefaghi, A. Rashidi, H. Ahmadi, S. Mohtasebi, M. Pourkhalil, Thermal and rheological properties of oil-based nanofluids from different carbon nanostructures, Int. Commun. Heat Mass 48 (2013) 178-182.

[42] E.J. Wasp, J.P. Kenny, R.L. Gandhi, Solid-liquid flow slurry pipeline transportation, Ser Bulk Mater Handl 1:56-58, 1977.

[43] B.C. Pak, Y.I. Cho, Hydrodynamic and heat transfer study of dispersed fluids with submicron metallic oxide particles, Exp. Heat Transf. Int. 11 (1998) 151-170.

[44] P.C. Mishra, S. Mukherjee, S.K. Nayak, A. Panda, A brief review on viscosity of nanofluids, Int. Nano Lett. 4 (2014) 109-120.

[45] A. Einstein, Eine neue bestimmung der moleküldimensionen, Ann. Phys. 324 (2) (1906) 289-306.

[46] R. Saito, M. Hofmann, G. Dresselhaus, A. Jorio, M.S. Dresselhaus, Raman spectroscopy of graphene and carbon nanotubes, Adv. Phys. 60 (2011) 413-550.

[47] H.C. Brinkman, The Viscosity of Concentrated Suspensions and Solutions, J. Chem. Phys. 20 (1952) 571-571.
[48] G.K. Batchelor, The effect of Brownian motion on the bulk stress in a suspension of spherical particles, J. Fluid Mech. 83 (1977) 97-117.
[49] H. Chen, Y. Ding, C. Tan, Rheological behaviour of nanofluids, New J. Phys. 9 (2007) 367.
[50] X. Wang, X. Xu, S.U. S. Choi, Thermal Conductivity of Nanoparticle - Fluid Mixture, J. Thermophys. Heat Trans. 13 (1999) 474-480.
[51] A. Dalkilic, A. Çebi, A. Celen, O. Yıldız, O. Acikgoz, C. Jumpholkul, M. Bayrak, K. Surana, S. Wongwises, Prediction of graphite nanofluids' dynamic viscosity by means of artificial neural networks, Int. Commun. Heat Mass 73 (2016) 33-42.
[52] A. Ghozatloo, S. Azimi Maleki, M. Shariaty-Niassar, A. Morad Rashidi, Investigation of Nanoparticles Morphology on Viscosity of Nanofluids and New Correlation for Prediction, J. Nanostruct. 5 (2015) 161-168.
[53] N. Saitô, Concentration Dependence of the Viscosity of High Polymer Solutions. I, J. Phys. Soc. Japan 5 (1950) 4-8.

Table 1
Source and mole fraction purity of the samples used in this work.

Chemical Name	Source	Mole Fraction Purity[a]	Analysis Method
PAO6	Repsol	> 0.99	NMR
ZrO_2 nanoparticles	Iolitec	0.999	ICP-AES
BN nanoparticles	Iolitec	0.99	XRF
Graphene nanoplatelets	Iolitec	0.995	Loss of Ignition and Raman

[a] Determined by the supplier.

Table 2
Experimental densities, ρ, determined with Stabinger SVM 3000 and DSA 5000 densimeters for PAO6 at several temperatures, T[a], and 0.0991 MPa[b].

T/K	ρ/g·cm^{-3}	T/K	ρ/g·cm^{-3}	T/K	ρ/g·cm^{-3}
			SVM 3000[c]		
278.15	0.8326	313.15	0.8111	348.15	0.7893
283.15	0.8295	318.15	0.8081	353.15	0.7861
288.15	0.8265	323.15	0.8050	358.15	0.7830
293.15	0.8235	328.15	0.8018	363.15	0.7799
298.15	0.8204	333.15	0.7987	368.15	0.7767
303.15	0.8173	338.15	0.7956	373.15	0.7736
308.15	0.8142	343.15	0.7924		
			DSA 5000[d]		
283.15	0.83008	303.15	0.81755	323.15	0.80505
288.15	0.82696	308.15	0.81442	328.15	0.80194
293.15	0.82382	313.15	0.81130	333.15	0.79884
298.15	0.82069	318.15	0.80817	338.15	0.79573

[a] Expanded temperature uncertainty is U(T) = 0.02 K; [b] expanded pressure uncertainty is U (p) = 0.0005 MPa; [c] combined expanded density uncertainty is U_c (ρ)= $5\cdot10^{-4}$ g·cm^{-3} and [d] combined expanded density uncertainty is U_c (ρ)= $4\cdot10^{-4}$ g·cm^{-3} (0.95 level of confidence).

Table 3
Experimental densities, ρ^a, determined with the Stabinger densimeter for the nanolubricants at several temperatures, T^b, and 0.0991 MPa[c].

T/K	ρ/g·cm^{-3}	T/K	ρ/g·cm^{-3}	T/K	ρ/g·cm^{-3}
99.5 wt% PAO6 + 0.5 wt% ZrO_2					
278.15	0.8357	313.15	0.8146	348.15	0.7937
283.15	0.8327	318.15	0.8116	353.15	0.7907
288.15	0.8297	323.15	0.8087	358.15	0.7876
293.15	0.8266	328.15	0.8057	363.15	0.7846
298.15	0.8236	333.15	0.8028	368.15	0.7815
303.15	0.8206	338.15	0.7998	373.15	0.7785
308.15	0.8175	343.15	0.7968		
99 wt% PAO6 + 1 wt% ZrO_2					
278.15	0.8397	313.15	0.8187	348.15	0.7985
283.15	0.8367	318.15	0.8165	353.15	0.7953
288.15	0.8336	323.15	0.8136	358.15	0.7923
293.15	0.8306	328.15	0.8107	363.15	0.7892
298.15	0.8275	333.15	0.8077	368.15	0.7861
303.15	0.8245	338.15	0.8046	373.15	0.7830
308.15	0.8215	343.15	0.8016		
98 wt% PAO6 + 2 wt% ZrO_2					
278.15	0.8475	313.15	0.8260	348.15	0.8044
283.15	0.8445	318.15	0.8230	353.15	0.8012
288.15	0.8415	323.15	0.8199	358.15	0.7981
293.15	0.8384	328.15	0.8168	363.15	0.7950
298.15	0.8353	333.15	0.8136	368.15	0.7919
303.15	0.8322	338.15	0.8105	373.15	0.7888
308.15	0.8291	343.15	0.8074		
99.95 wt% PAO6 + 0.05 wt% GnP					
278.15	0.8332	313.15	0.8119	348.15	0.7902
283.15	0.8302	318.15	0.8088	353.15	0.7870
288.15	0.8272	323.15	0.8057	358.15	0.7839
293.15	0.8241	328.15	0.8026	363.15	0.7808
298.15	0.8211	333.15	0.7995	368.15	0.7777
303.15	0.8180	338.15	0.7964	373.15	0.7745
308.15	0.8149	343.15	0.7933		
99.9 wt% PAO6 + 0.1 wt% GnP					
278.15	0.8335	313.15	0.8121	348.15	0.7905

283.15	0.8304	318.15	0.8090	353.15	0.7874
288.15	0.8274	323.15	0.8059	358.15	0.7843
293.15	0.8243	328.15	0.8029	363.15	0.7812
298.15	0.8213	333.15	0.7998	368.15	0.7781
303.15	0.8182	338.15	0.7967	373.15	0.7750
308.15	0.8152	343.15	0.7936		
99.75 wt% PAO6 + 0.25 wt% GnP					
278.15	0.8341	313.15	0.8128	348.15	0.7915
283.15	0.8311	318.15	0.8097	353.15	0.7883
288.15	0.8280	323.15	0.8067	358.15	0.7852
293.15	0.8250	328.15	0.8037	363.15	0.7821
298.15	0.8219	333.15	0.8007	368.15	0.7790
303.15	0.8189	338.15	0.7976	373.15	0.7759
308.15	0.8158	343.15	0.7946		
99.95 wt% PAO6 + 0.05 wt% BN					
278.15	0.8332	313.15	0.8119	348.15	0.7902
283.15	0.8302	318.15	0.8088	353.15	0.7871
288.15	0.8272	323.15	0.8058	358.15	0.7840
293.15	0.8241	328.15	0.8027	363.15	0.7809
298.15	0.8211	333.15	0.7996	368.15	0.7778
303.15	0.8180	338.15	0.7965	373.15	0.7747
308.15	0.8150	343.15	0.7934		
99.9 wt% PAO6 + 0.1 wt% BN					
278.15	0.8338	313.15	0.8125	348.15	0.7909
283.15	0.8308	318.15	0.8094	353.15	0.7878
288.15	0.8278	323.15	0.8063	358.15	0.7846
293.15	0.8247	328.15	0.8033	363.15	0.7815
298.15	0.8216	333.15	0.8002	368.15	0.7784
303.15	0.8186	338.15	0.7971	373.15	0.7753
308.15	0.8155	343.15	0.7940		
99.75 wt% PAO6 + 0.25 wt% BN					
278.15	0.8346	313.15	0.8132	348.15	0.7914
283.15	0.8315	318.15	0.8101	353.15	0.7883
288.15	0.8285	323.15	0.8070	358.15	0.7851
293.15	0.8254	328.15	0.8039	363.15	0.7820
298.15	0.8224	333.15	0.8008	368.15	0.7789
303.15	0.8193	338.15	0.7977	373.15	0.7758

308.15	0.8162	343.15	0.7945

[a] Combined expanded density uncertainty is U_c (ρ)= $5 \cdot 10^{-4}$ g·cm^{-3}; [b] expanded temperature uncertainty is U(T) = 0.02 K and [c] expanded pressure uncertainty is U (p) = 0.0005 MPa (0.95 level of confidence).

Table 4

Experimental densities, ρ^{a}, determined with DSA 5000 for the nanolubricants at different temperatures, T[b], and 0.0991 MPa[c].

T/K	ρ/g·cm^{-3}	T/K	ρ/g·cm^{-3}	T/K	ρ/g·cm^{-3}
99.5 wt% PAO6 + 0.5 wt% ZrO_2					
283.15	0.83327	303.15	0.82076	323.15	0.80830
288.15	0.83015	308.15	0.81764	328.15	0.80521
293.15	0.82702	313.15	0.81452	333.15	0.80213
298.15	0.82388	318.15	0.81140	338.15	0.79905
99 wt% PAO6 + 1 wt% ZrO_2					
283.15	0.83741	303.15	0.82490	323.15	0.81242
288.15	0.83428	308.15	0.82177	328.15	0.80932
293.15	0.83115	313.15	0.81865	333.15	0.80615
298.15	0.82802	318.15	0.81553	338.15	0.80316
98 wt% PAO6 + 2 wt% ZrO_2					
283.15	0.84414	303.15	0.83168	323.15	0.81922
288.15	0.84104	308.15	0.82856	328.15	0.81612
293.15	0.83792	313.15	0.82544	333.15	0.81303
298.15	0.83480	318.15	0.82233	338.15	0.80995
99.95 wt% PAO6 + 0.05 wt% GnP					
283.15	0.83032	303.15	0.81778	323.15	0.80527
288.15	0.82720	308.15	0.81465	328.15	0.80215
293.15	0.82406	313.15	0.81152	333.15	0.79904
298.15	0.82092	318.15	0.80839	338.15	0.79593
99.9 wt% PAO6 + 0.1 wt% GnP					
283.15	0.83062	303.15	0.81809	323.15	0.80557
288.15	0.82750	308.15	0.81495	328.15	0.80245
293.15	0.82436	313.15	0.81182	333.15	0.79933
298.15	0.82122	318.15	0.80869	338.15	0.79621
99.75 wt% PAO6 + 0.25 wt% GnP					
283.15	0.83132	303.15	0.81878	323.15	0.80627
288.15	0.82820	308.15	0.81565	328.15	0.80315
293.15	0.82505	313.15	0.81252	333.15	0.80004
298.15	0.82191	318.15	0.80939	338.15	0.79693
99.95 wt% PAO6 + 0.05 wt% BN					
283.15	0.83040	303.15	0.81787	323.15	0.80536
288.15	0.82728	308.15	0.81474	328.15	0.80225
293.15	0.82414	313.15	0.81161	333.15	0.79914
298.15	0.82100	318.15	0.80848	338.15	0.79604
99.9 wt% PAO6 + 0.1 wt% BN					

283.15	0.83095	303.15	0.81842	323.15	0.80591
288.15	0.82782	308.15	0.81528	328.15	0.80280
293.15	0.82469	313.15	0.81216	333.15	0.79969
298.15	0.82155	318.15	0.80903	338.15	0.79658
		99.75 wt% PAO6 + 0.25 wt% BN			
283.15	0.83130	303.15	0.81876	323.15	0.80625
288.15	0.82817	308.15	0.81563	328.15	0.80313
293.15	0.82503	313.15	0.81250	333.15	0.80002
298.15	0.82190	318.15	0.80938	338.15	0.79691

[a] Combined expanded density uncertainty is U_c (ρ)= $4 \cdot 10^{-4}$ g·cm^{-3}; [b] expanded temperature uncertainty is U(T) = 0.02 K and [c] expanded pressure uncertainty is U (p) = 0.0005 MPa (0.95 level of confidence).

Table 5
Experimental sound velocity, u^a, determined with DSA 5000 for the oil base fluid (PAO6) and the nanolubricants at 0.0991 MPa[b] at different temperatures T^c.

T^c/K	u/m·s^{-1}	T/K	u/m·s^{-1}	T/K	u/m·s^{-1}
PAO6 base oil					
283.15	1465.9	303.15	1394.4	323.15	1326.4
288.15	1447.7	308.15	1377.1	328.15	1310.1
293.15	1429.8	313.15	1359.9	333.15	1293.8
298.15	1411.9	318.15	1343.1	338.15	1277.8
99.5 wt% PAO6 + 0.5 wt% ZrO_2					
283.15	1464.3	303.15	1393.6	323.15	1326.1
288.15	1446.2	308.15	1376.4	328.15	1309.7
293.15	1428.4	313.15	1359.5	333.15	1293.5
298.15	1410.9	318.15	1342.7	338.15	1277.7
99 wt% PAO6 + 1 wt% ZrO_2					
283.15	1461.1	303.15	1396.3	323.15	1329.2
288.15	1445.5	308.15	1378.4	328.15	1313.7
293.15	1429.7	313.15	1361.2	333.15	1295.4
298.15	1413.4	318.15	1344.7	338.15	1279.1
98 wt% PAO6 + 2 wt% ZrO_2					
283.15	1457.4	303.15	1386.9	323.15	1320.9
288.15	1439.1	308.15	1370.2	328.15	1304.8
293.15	1421.2	313.15	1353.7	333.15	1288.9
298.15	1403.9	318.15	1337.3	338.15	1273.3
99.95 wt% PAO6 + 0.05 wt% GnP					
283.15	1465.8	303.15	1394.2	323.15	1326.1
288.15	1447.6	308.15	1376.9	328.15	1309.7
293.15	1429.7	313.15	1359.7	333.15	1293.3
298.15	1411.8	318.15	1342.8	338.15	1277.3
99.9 wt% PAO6 + 0.1 wt% GnP					
283.15	1465.7	303.15	1394.1	323.15	1325.7
288.15	1447.5	308.15	1376.7	328.15	1309.2
293.15	1429.5	313.15	1359.5	333.15	1292.7
298.15	1411.7	318.15	1342.5	338.15	1276.5
99.75 wt% PAO6 + 0.25 wt% GnP					
283.15	1465.5	303.15	1393.9	323.15	1325.7
288.15	1447.3	308.15	1376.5	328.15	1309.2
293.15	1429.3	313.15	1359.3	333.15	1292.9
298.15	1411.5	318.15	1342.4	338.15	1276.9
99.95 wt% PAO6 + 0.05 wt% BN					

283.15	1465.5	303.15	1393.9	323.15	1325.5
288.15	1447.4	308.15	1376.5	328.15	1308.9
293.15	1429.4	313.15	1359.4	333.15	1292.4
298.15	1411.5	318.15	1342.4	338.15	1276.1
		99.9 wt% PAO6 + 0.1 wt% BN			
283.15	1465.6	303.15	1394.1	323.15	1325.9
288.15	1447.5	308.15	1376.7	328.15	1309.3
293.15	1429.5	313.15	1359.6	333.15	1292.9
298.15	1411.7	318.15	1342.6	338.15	1276.7
		99.75 wt% PAO6 + 0.25 wt% BN			
283.15	1465.6	303.15	1394.1	323.15	1325.8
288.15	1447.5	308.15	1376.7	328.15	1309.2
293.15	1429.4	313.15	1359.5	333.15	1292.8
298.15	1411.7	318.15	1342.5	338.15	1276.5

[a] Combined expanded speed of sound uncertainty is U_c (u)= 4·m·s^{-1}; [b] expanded pressure uncertainty is U (p) = 0.0005 MPa and [c] expanded temperature uncertainty is U(T) = 0.02 K (0.95 level of confidence).

Table 6
Experimental viscosity, η^a, determined with Stabinger rotational viscometer for the base oil (PAO6) and the nanolubricants at 0.0991 MPa[b] at different temperatures T^c.

T^c/K	η/mPa·s	T/K	η/mPa·s	T/K	η/mPa·s
PAO6 base oil					
278.15	133.4	313.15	24.14	348.15	7.907
283.15	99.32	318.15	19.99	353.15	6.959
288.15	75.46	323.15	16.74	358.15	6.162
293.15	58.33	328.15	14.16	363.15	5.492
298.15	45.79	333.15	12.09	368.15	4.917
303.15	36.50	338.15	10.41	373.15	4.426
308.15	29.49	343.15	9.038		
99.5 wt% PAO6 + 0.5 wt% ZrO_2					
278.15	136.3	313.15	24.49	348.15	7.982
283.15	101.2	318.15	20.27	353.15	7.028
288.15	76.76	323.15	16.96	358.15	6.225
293.15	59.27	328.15	14.34	363.15	5.551
298.15	46.52	333.15	12.21	368.15	4.969
303.15	37.06	338.15	10.52	373.15	4.473
308.15	29.94	343.15	9.129		
99 wt% PAO6 + 1 wt% ZrO_2					
278.15	137.9	313.15	24.75	348.15	8.071
283.15	102.4	318.15	20.49	353.15	7.101
288.15	77.62	323.15	17.15	358.15	6.286
293.15	59.91	328.15	14.51	363.15	5.595
298.15	47.00	333.15	12.36	368.15	5.013
303.15	37.44	338.15	10.64	373.15	4.508
308.15	30.25	343.15	9.235		
98 wt% PAO6 + 2 wt% ZrO_2					
278.15	145.4	313.15	25.84	348.15	8.324
283.15	108.0	318.15	21.37	353.15	7.321
288.15	81.75	323.15	17.86	358.15	6.483
293.15	63.01	328.15	15.04	363.15	5.775
298.15	49.34	333.15	12.81	368.15	5.175
303.15	39.23	338.15	11.00	373.15	4.655
308.15	31.67	343.15	9.534		
99.95 wt% PAO6 + 0.05 wt% GnP					
278.15	134.8	313.15	24.40	348.15	7.979

283.15	100.3	318.15	20.21	353.15	7.021
288.15	76.22	323.15	16.93	358.15	6.216
293.15	58.89	328.15	14.31	363.15	5.523
298.15	46.31	333.15	12.21	368.15	4.949
303.15	36.88	338.15	10.52	373.15	4.453
308.15	29.82	343.15	9.127		
99.9 wt% PAO6+ 0.1 wt% GnP					
278.15	136.2	313.15	24.66	348.15	8.093
283.15	101.4	318.15	20.44	353.15	7.125
288.15	77.03	323.15	17.13	358.15	6.313
293.15	59.52	328.15	14.50	363.15	5.629
298.15	46.74	333.15	12.37	368.15	5.049
303.15	37.25	338.15	10.65	373.15	4.539
308.15	30.11	343.15	9.251		
99.75 wt% PAO6 + 0.25 wt% GnP					
278.15	140.1	313.15	25.31	348.15	8.277
283.15	104.3	318.15	20.98	353.15	7.282
288.15	79.13	323.15	17.56	358.15	6.444
293.15	61.12	328.15	14.84	363.15	5.741
298.15	47.98	333.15	12.67	368.15	5.146
303.15	38.24	338.15	10.91	373.15	4.627
308.15	30.91	343.15	9.464		
99.95 wt% PAO6 + 0.05 wt% BN					
278.15	134.6	313.15	24.30	348.15	7.942
283.15	100.1	318.15	20.13	353.15	6.989
288.15	75.98	323.15	16.86	358.15	6.190
293.15	58.75	328.15	14.26	363.15	5.516
298.15	46.15	333.15	12.15	368.15	4.940
303.15	36.75	338.15	10.47	373.15	4.445
308.15	29.70	343.15	9.085		
99.9 wt% PAO6 + 0.1 wt% BN					
278.15	135.7	313.15	24.46	348.15	7.966
283.15	100.8	318.15	20.26	353.15	7.008
288.15	76.60	323.15	16.95	358.15	6.202
293.15	59.27	328.15	14.32	363.15	5.519
298.15	46.51	333.15	12.21	368.15	4.938
303.15	37.04	338.15	10.51	373.15	4.444
308.15	29.87	343.15	9.117		
99.75 wt% PAO6 + 0.25 wt% BN					

278.15	136.9	313.15	24.59	348.15	8.025
283.15	101.8	318.15	20.33	353.15	7.067
288.15	77.23	323.15	17.02	358.15	6.262
293.15	59.62	328.15	14.40	363.15	5.584
298.15	46.75	333.15	12.29	368.15	5.007
303.15	37.24	338.15	10.57	373.15	4.508
308.15	30.06	343.15	9.177		

[a] Combined relative expanded viscosity uncertainty is U_c (η) = 1%; [b] expanded pressure uncertainty is U (p) = 0.0005 MPa and [c] expanded temperature uncertainty is U(T) = 0.02 K (0.95 level of confidence).

Table 7
Parameters obtained (*A*, *B* and *C*) for Eq. (4) for PAO6 base oil and each nanolubricant and average absolute deviation (*AAD*%) between experimental and correlated viscosity values

Sample	***A* / mPa·s^{-1}**	***B* / K**	***C* / K**	***AAD*%**
PAO6 base oil	0.0333	1121.0	143.02	0.46
99.5 wt% PAO6 + 0.5 wt% ZrO_2	0.0347	1108.1	144.23	0.40
99 wt% PAO6 + 1 wt% ZrO_2	0.0360	1100.2	144.83	0.30
98 wt% PAO6 + 2 wt% ZrO_2	0.0320	1144.6	142.26	0.51
99.95 wt% PAO6 + 0.05 wt% GnP	0.0336	1121.6	142.99	0.37
99.9 wt% PAO6+ 0.1 wt% GnP	0.0358	1105.7	144.05	0.42
99.75 wt% PAO6 + 0.25 wt% GnP	0.0358	1111.5	143.78	0.36
99.95 wt% PAO6 + 0.05 wt% BN	0.0342	1113.9	143.61	0.38
99.9 wt% PAO6+ 0.1 wt% BN	0.0323	1132.2	142.43	0.40
99.75 wt% PAO6 + 0.25 wt% BN	0.0340	1116.3	143.67	0.52

Table 8

Theoretical models used for the prediction of density, ρ, and viscosity, η, of nanolubricants.

Density models	
Wasp *et al*. **[42]**	$\frac{1}{\rho_{nl}} = \frac{\varphi}{\rho_{np}} + \frac{1-\varphi}{\rho_{bf}}$
Pak and Cho **[43]**	$\rho_{nl} = \phi\rho_{np} + (1-\phi)\,\rho_{bf}$
Viscosity models	
Einstein **[45]**	$\eta_{nl} = (1+2.5\phi)\,\eta_{bf}$
Saito **[53]**	$\eta_{nl} = (1+\frac{2.5\phi}{1-\phi})\,\eta_{bf}$
Brinkman **[47]**	$\eta_{nl} = (1-\phi)^{-2.5}\,\eta_{bf}$
Batchelor **[48]**	$\eta_{nl} = (1+2.5\phi+6.5\phi^2)\,\eta_{bf}$
Wang **[50]**	$\eta_{nl} = (1+7.3\phi+123\phi^2)\,\eta_{bf}$
Chen *et al*. **[49]**	$\eta_{nl} = (1+10.6\phi+(10.6\phi)^2)\,\eta_{bf}$

Subscripts *nl*, *np* and *bf* refers to nanolubricant, nanoparticle and base oil, respectively. Symbols φ and ϕ are the nanoadditive mass and volume fractions, respectively.

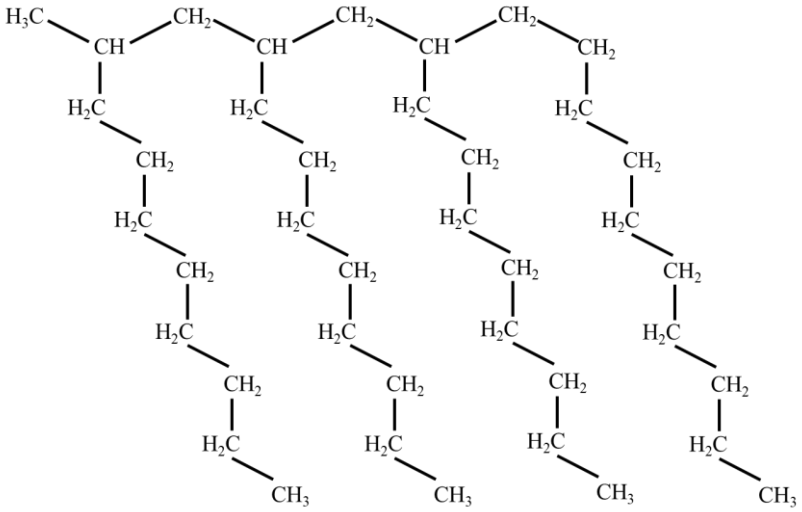

Fig. 1. Schematic representation of a typical linear tetramer of the polyalphaolefin synthetic base oil (PAO6).

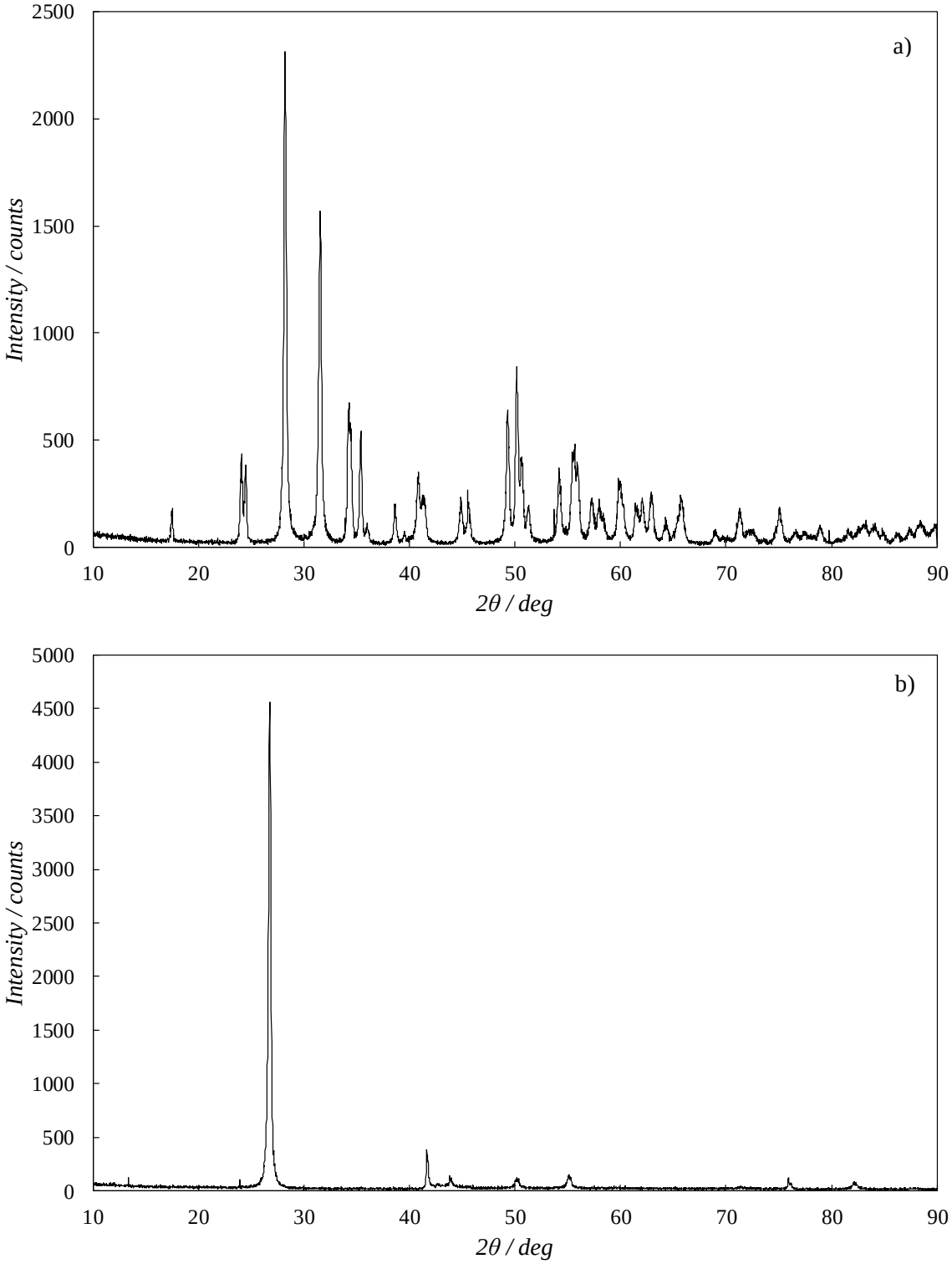

Fig. 2. X-ray patterns of the nanopowders of a) ZrO_2 and b) BN.

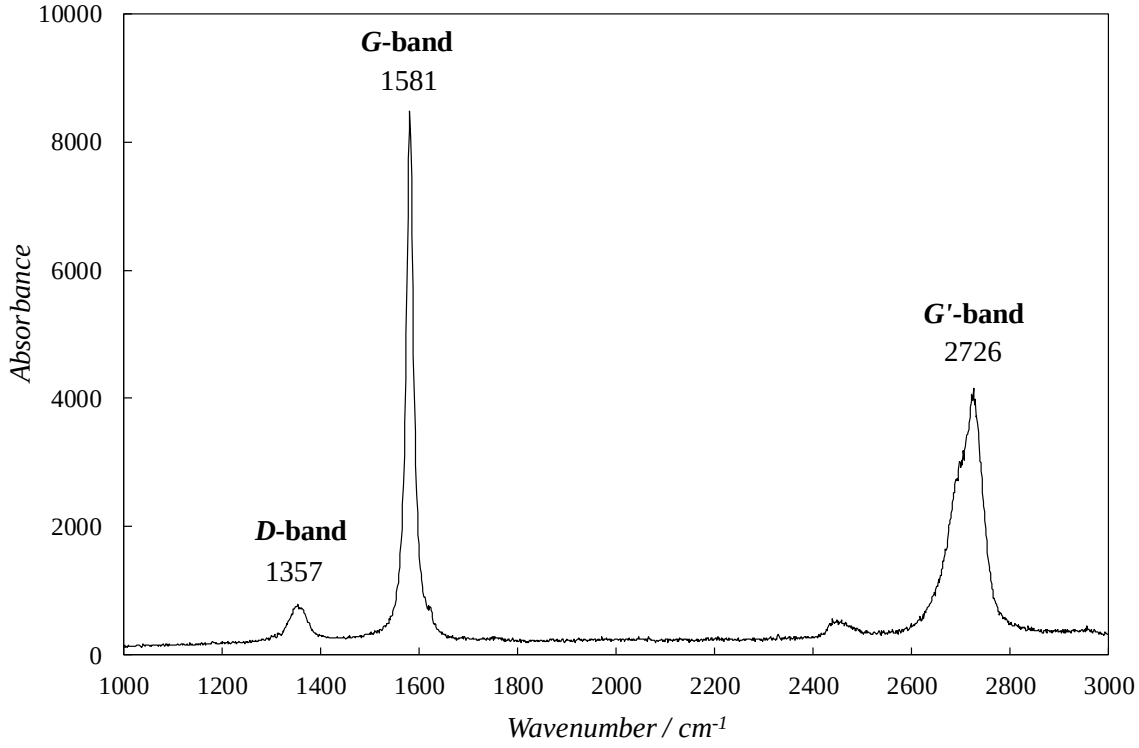

Fig. 3. Raman spectrum of graphene nanoplatelets.

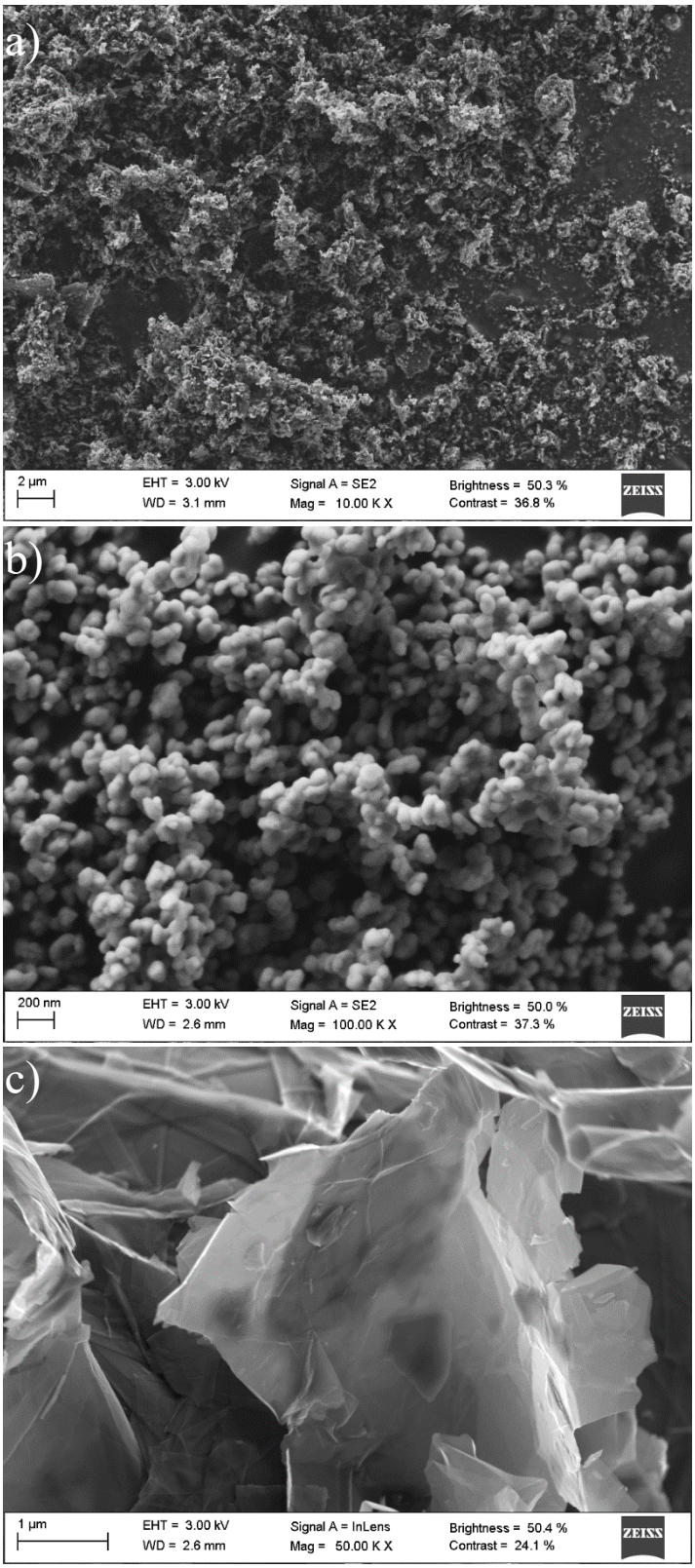

Fig. 4. SEM micrographs of three different nanoparticles: boron nitride nanoparticles (a), spherically shaped ZrO_2 nanoparticles (b) and graphene nanoplatelets (c).

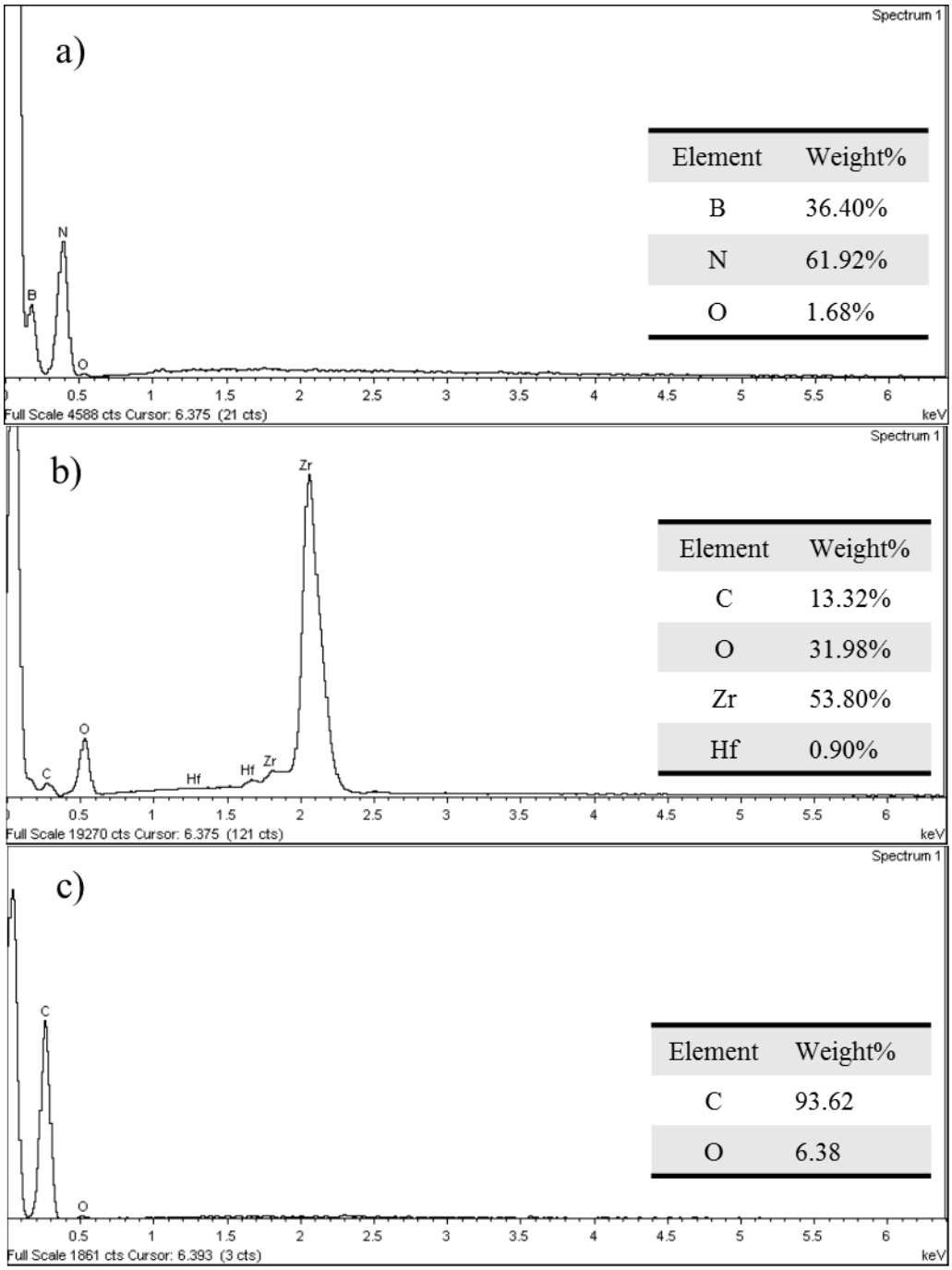

Fig. 5. EDX microanalyses: a) boron nitride nanoparticles, b) spherically shaped ZrO_2 nanoparticles and c) graphene nanoplatelets.

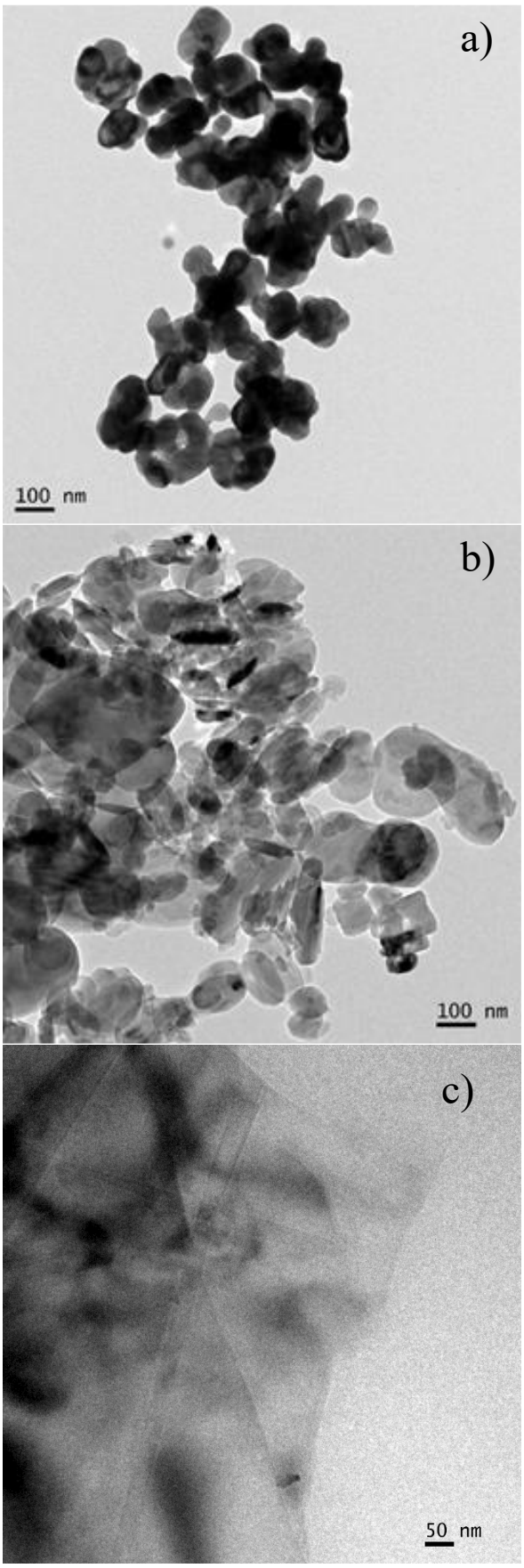

Fig. 6. TEM images showing aggregation: a) ZrO_2 nanoparticles, b) BN nanoparticles and c) graphene nanoplatelets dispersed in n-butanol.

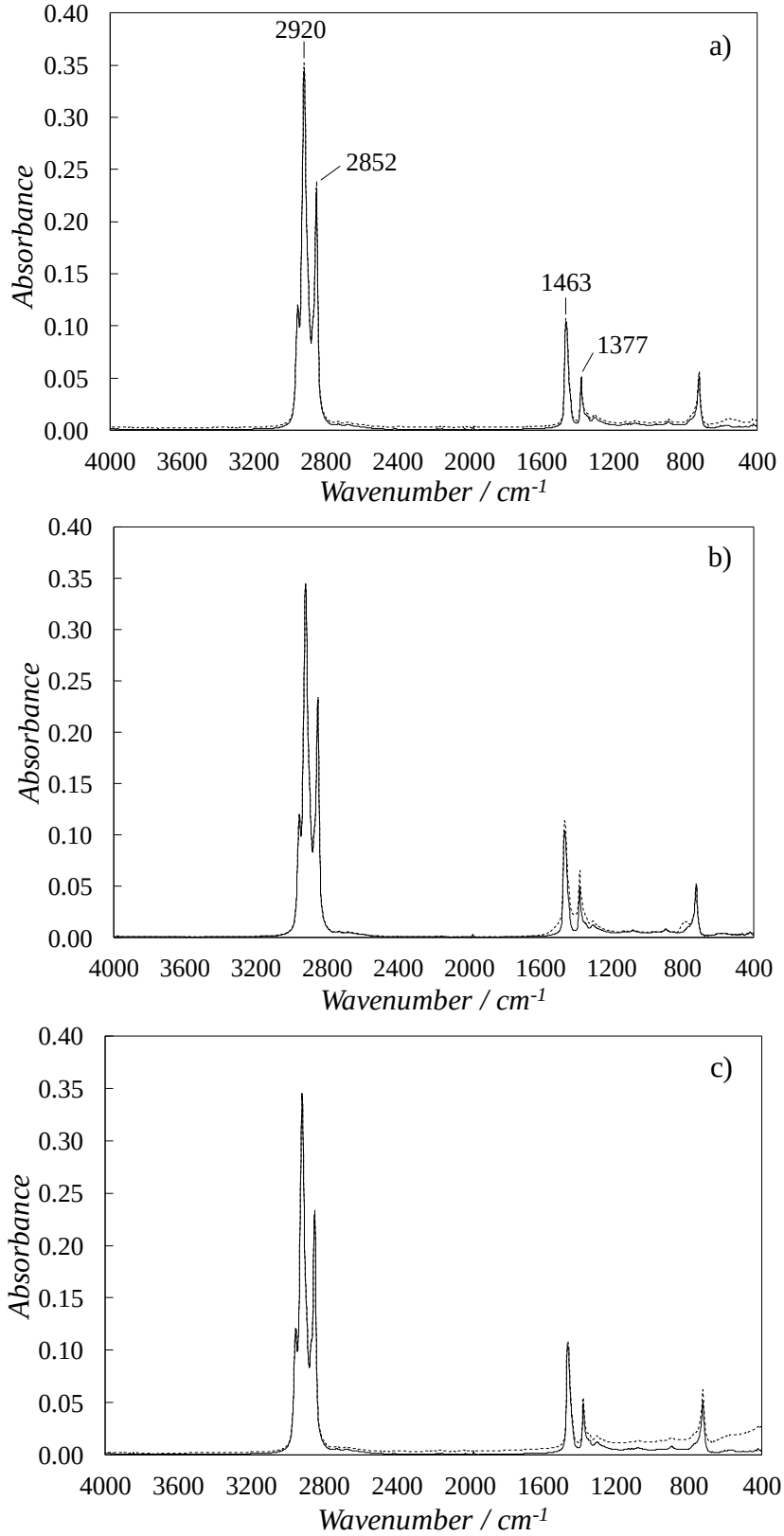

Fig. 7. FTIR spectra of base oil PAO6 (continuous line) and of nanolubricants (broken line): a) 2.0 wt% ZrO_2, b) 0.25 wt% BN and c) 0.25 wt% GnP.

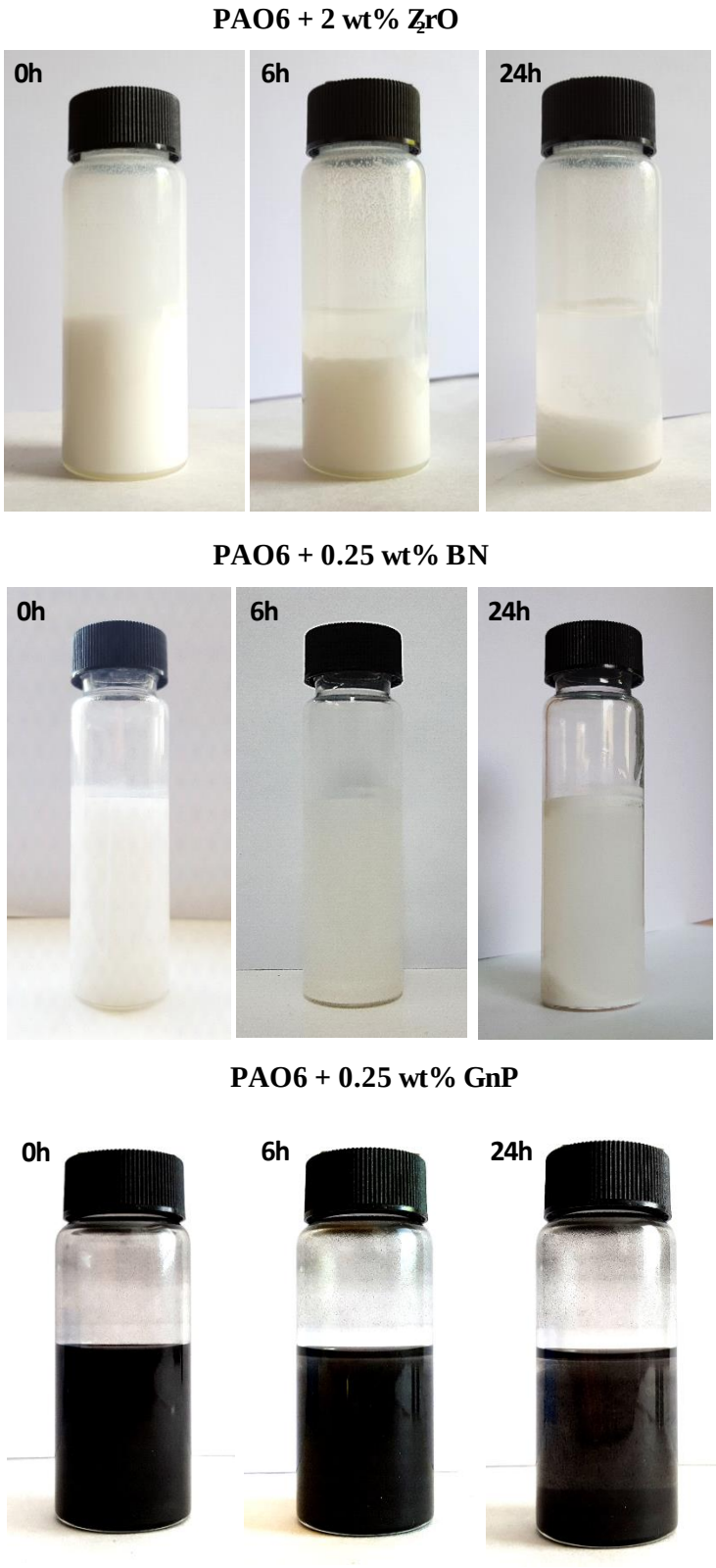

Fig. 8. Photographs to observe the sedimentation of nanoadditives in PAO6.

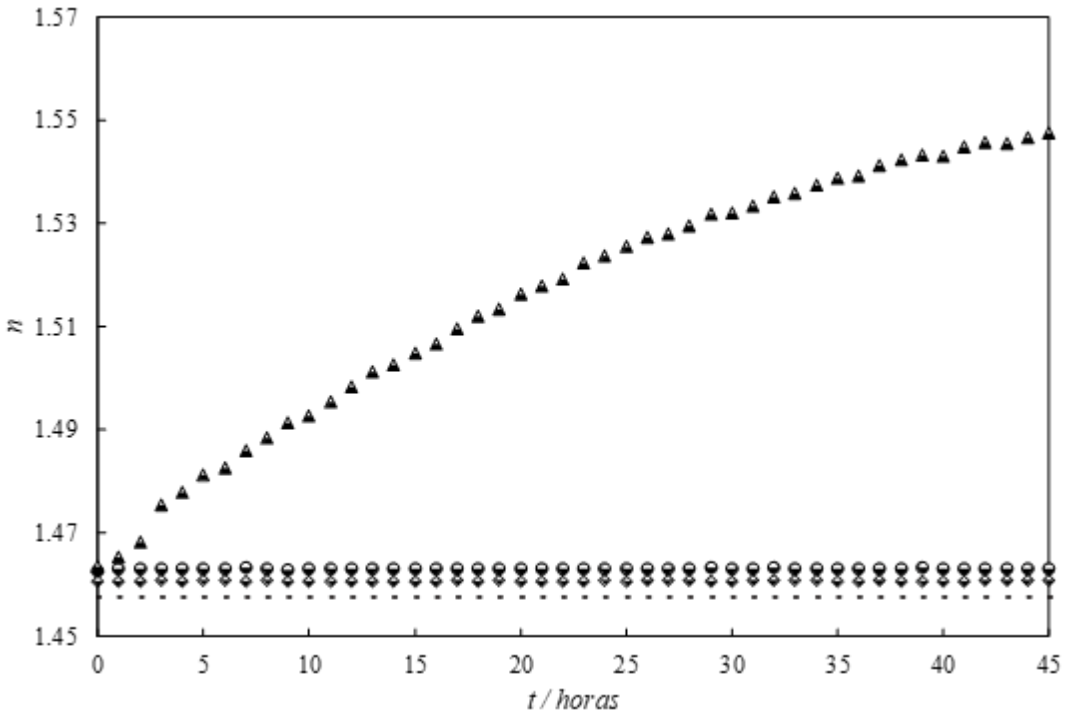

Fig. 9. Temporal evolution of the refractive index, *n*, at *T* = 298.15 K for base oil, PAO6 (broken line), and for nanolubricants at 2 wt%. ZrO_2 (triangle), 0.25 wt% BN (circle) and 0.25 wt% GnP (rhombus).

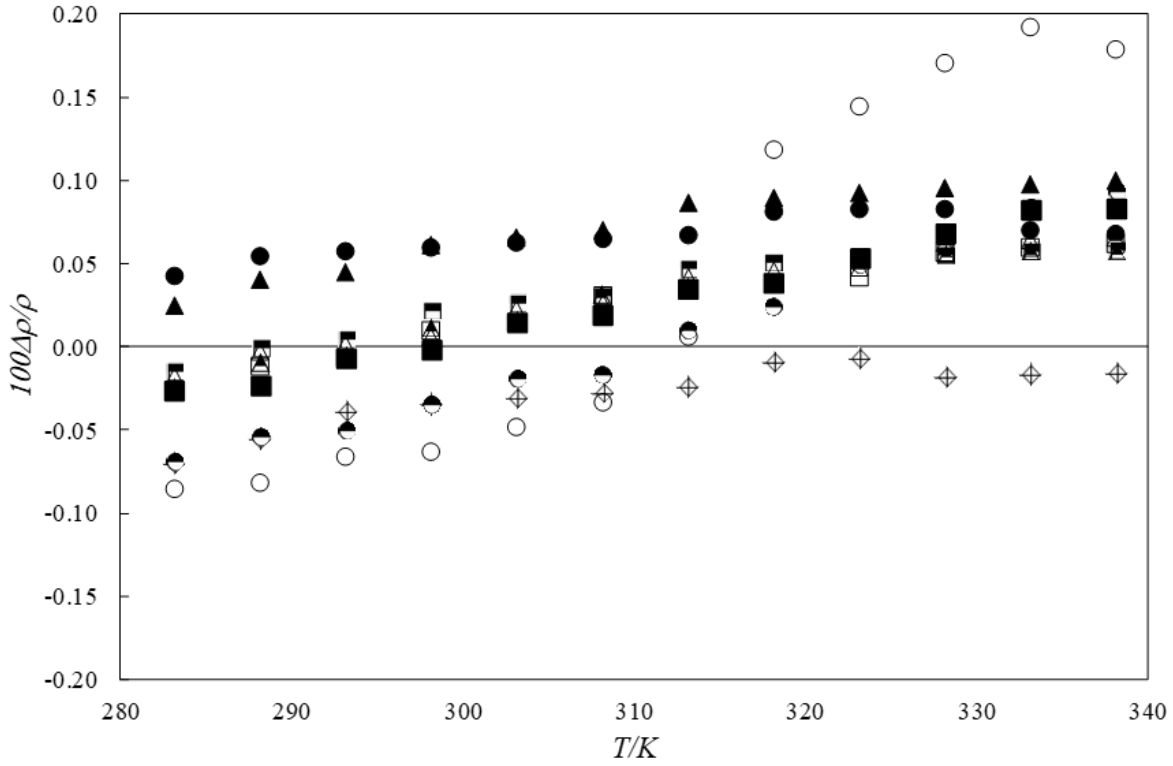

Fig. 10. Relative deviation between density values obtained with DSA 5000 and Anton Paar SVM 3000 Stabinger densimeters for ( ) base oil PAO6, ( ) 0.5 wt% ZrO_2, ( ) 1.0 wt% ZrO_2, ( ) 2.0 wt% ZrO_2, ( ) 0.05 wt% BN, ( ) 0.10 wt% BN, ( ) 0.25 wt% BN, ( ) 0.05 wt% GnP, ( ) 0.10 wt% GnP and ( ) 0.25 wt% GnP.

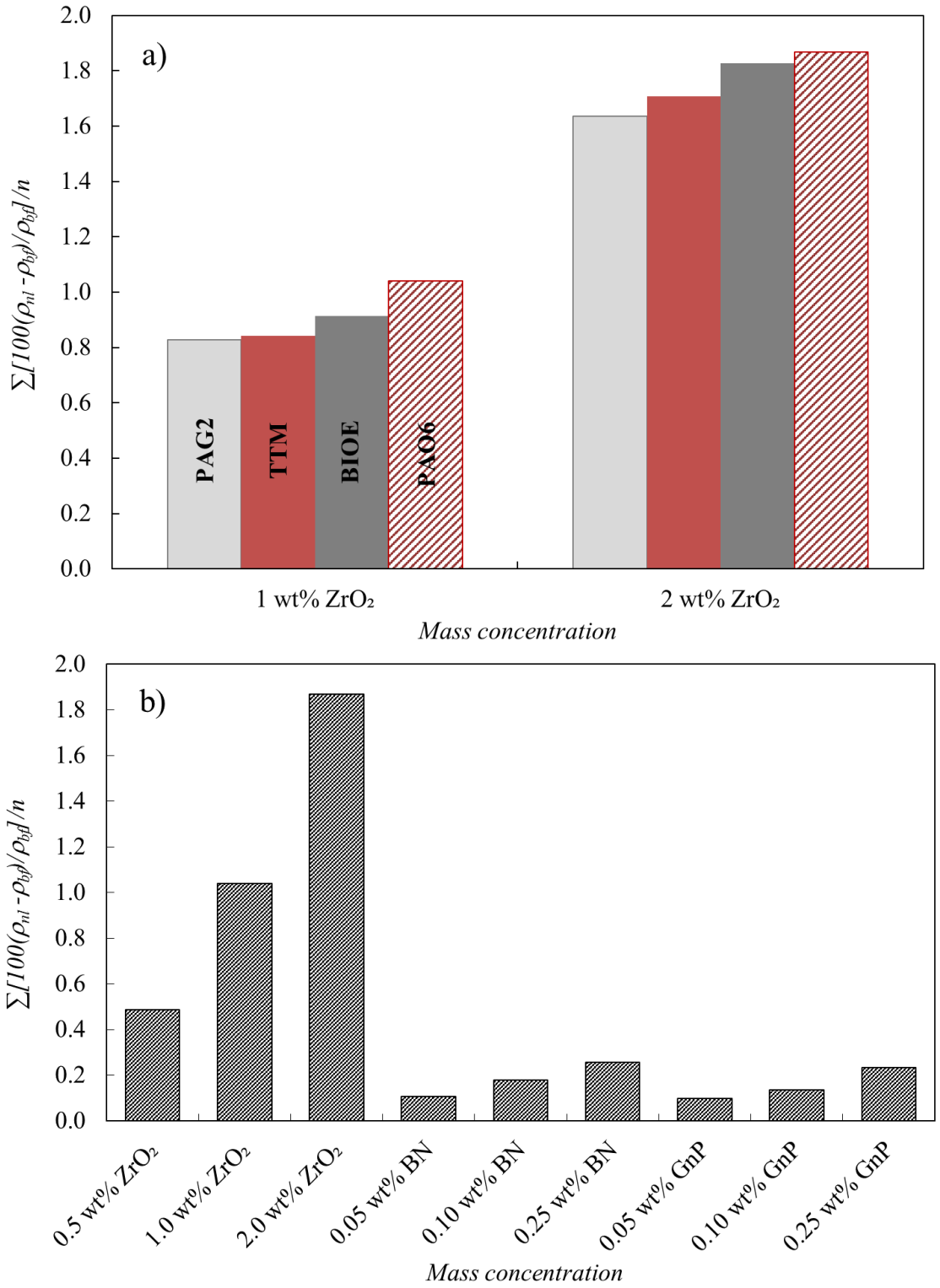

Fig. 11. Average relative deviations of the nanolubricant density (ρ_{nl}) with respect to the base oil (ρ_{bf}): (a) Comparison between PAO6/ZrO_2, studied in the present work, and TTM/ZrO_2, TTM/ZrO_2 and BIOE/ZrO_2 previously published [11] for the same mass concentration. (b) Results found in the present work using additives of different morphology.

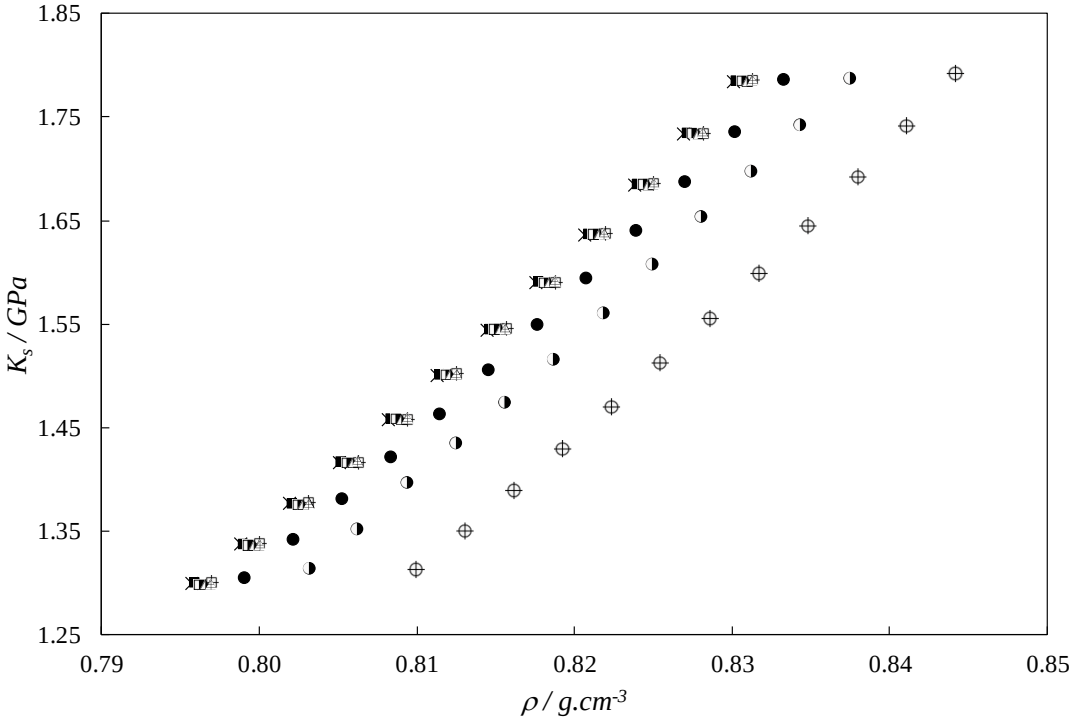

Fig. 12. Adiabatic bulk modulus, K_s, for each nanolubricant as a function of the density: (×) base oil PAO6, (●) 0.5wt% ZrO_2, (◑) 1.0wt% ZrO_2, (⊕) 2.0wt% ZrO_2, (▲) 0.05wt% BN, (◭) 0.10wt% BN, (⧋) 0.25wt% BN, (■) 0.05wt% GnP, (◧) 0.10wt% GnP and (⊞) 0.25wt% GnP.

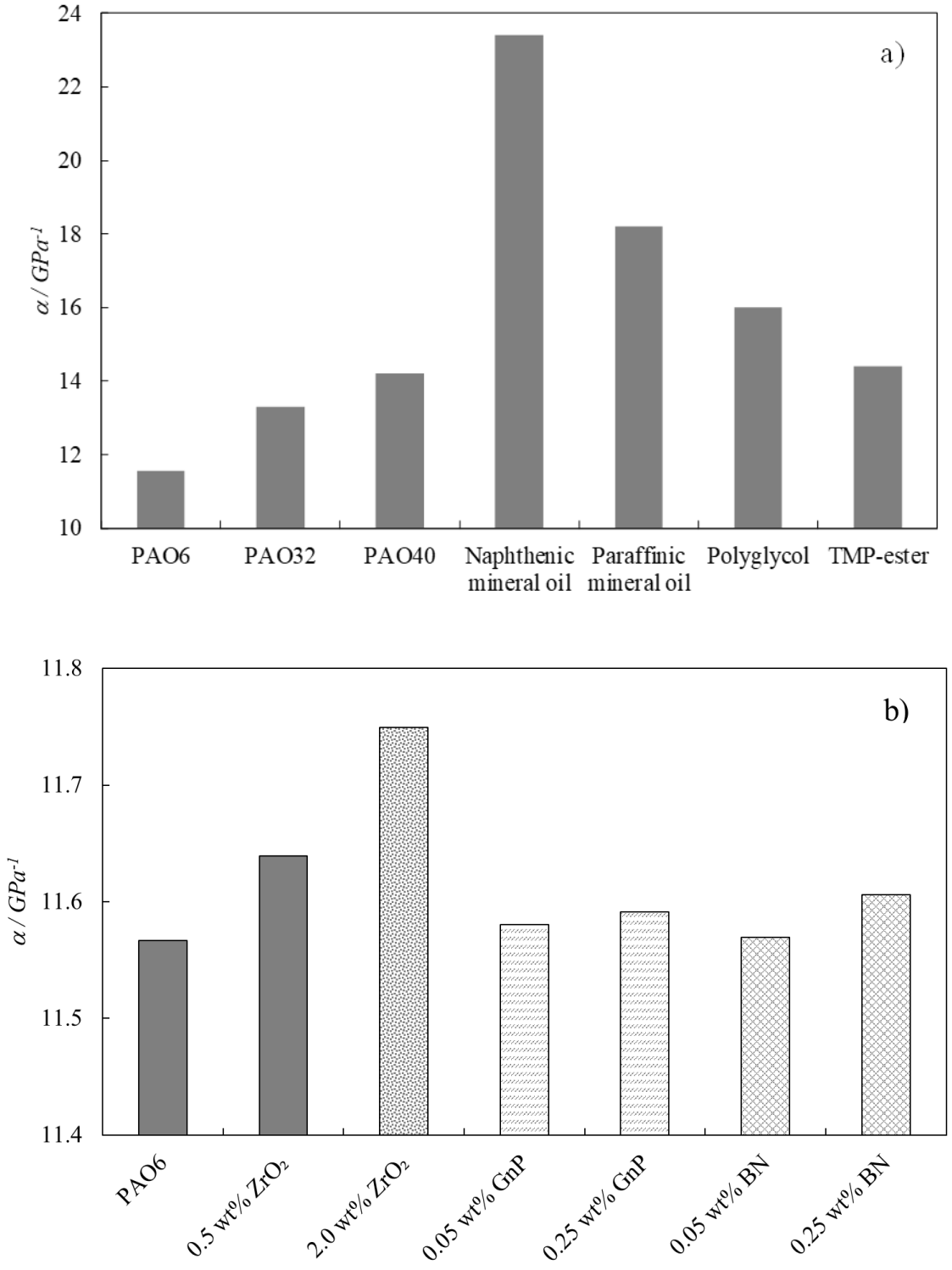

Fig. 13. Pressure-viscosity coefficient (α) at T = 313.15 K and 0.1 MPa: (a) for PAO6 and other polyalphaolefins [37] and other mineral and synthetic oils [38]; (b) for the base oil and several nanolubricants studied in this work.

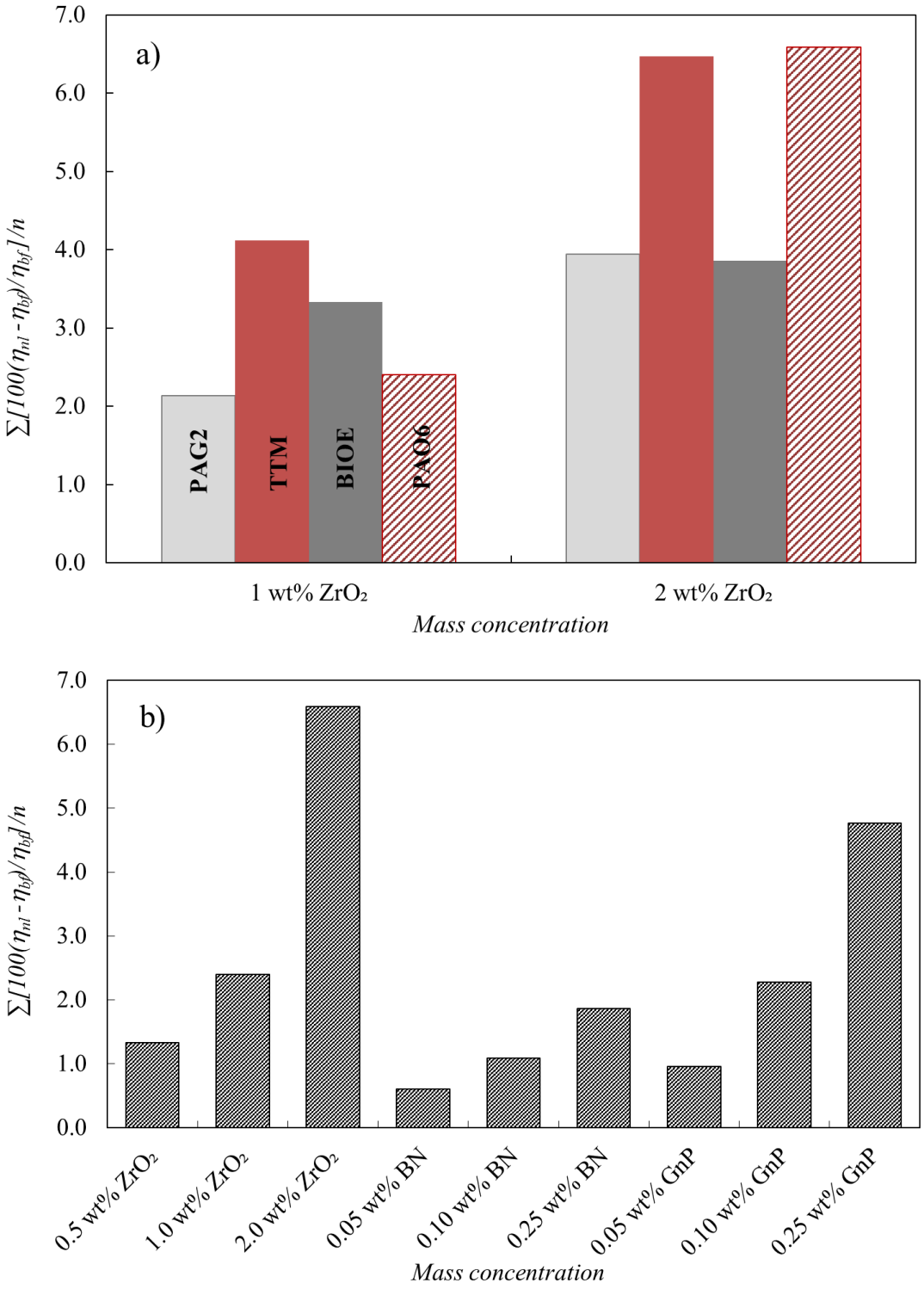

Fig. 14. Average relative deviations of the nanolubricant viscosity (η_{nl}) with respect to the base oil (η_{bf}): (a) Comparison between PAO6/ZrO_2, studied in the present work, and TTM/ZrO_2, TTM/ZrO_2 and BIOE/ZrO_2 previously published [11] for the same mass concentration. (b) Results found in the present work using additives of different morphology.

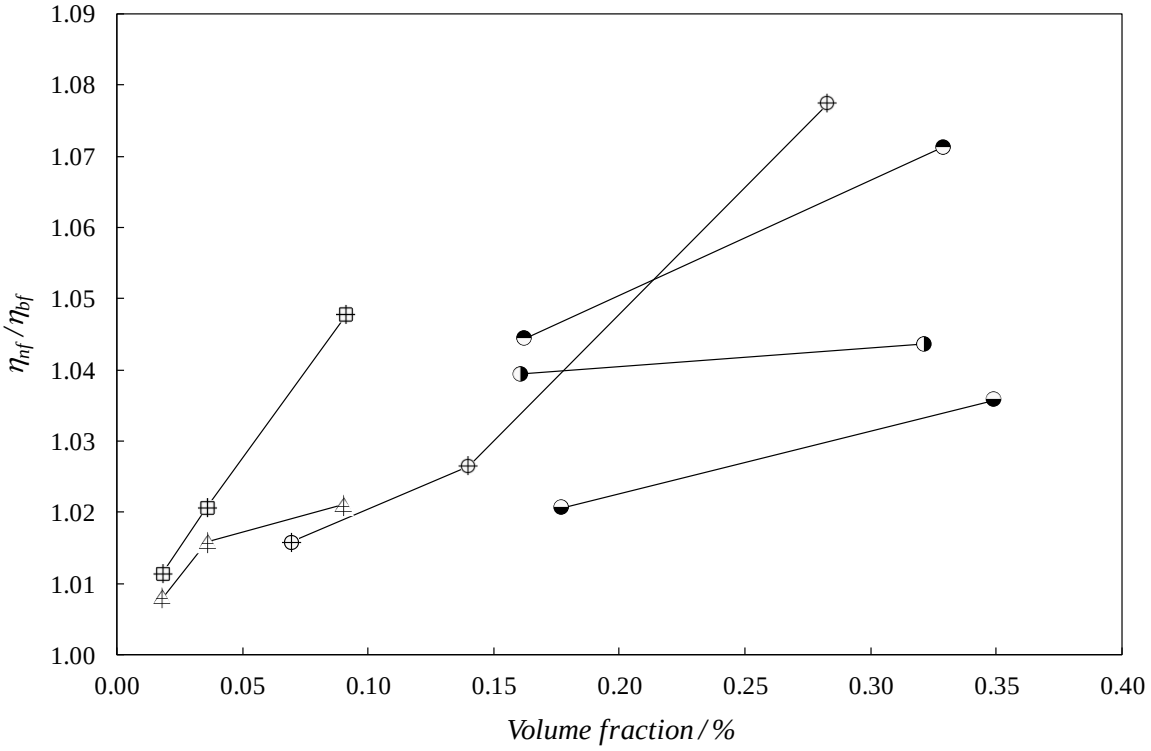

Fig. 15. Variation of relative dynamic viscosity obtained in the present work for: (⊕) PAO6/ZrO_2, (⧋) PAO6/BN and (⊞) PAO6/GnP at T = 298.15 K. Values previously obtained [11] for (◒) PAG2/ZrO_2, (◓) TTM/ ZrO_2 and (◑) BIOE/ ZrO_2.

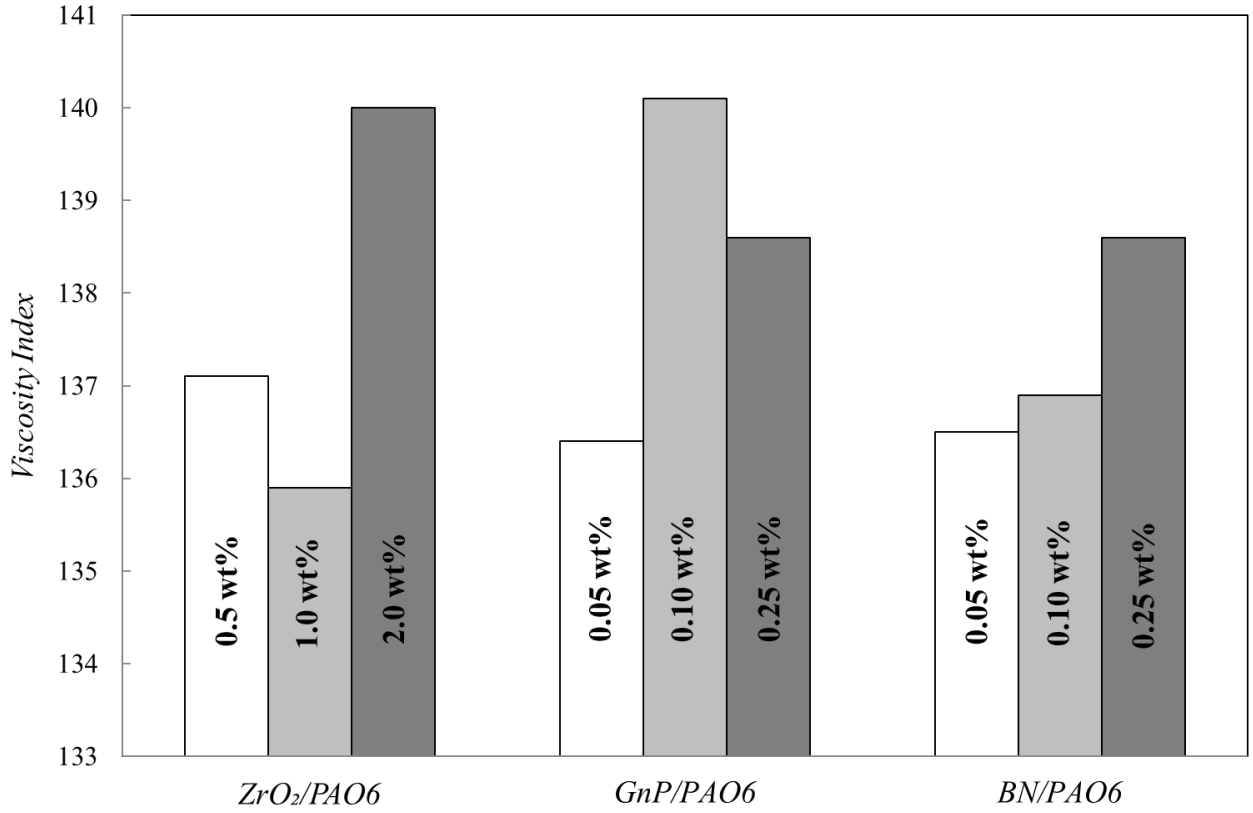

Fig. 16. Viscosity index, *VI*, for all the nanolubricants based on PAO6.

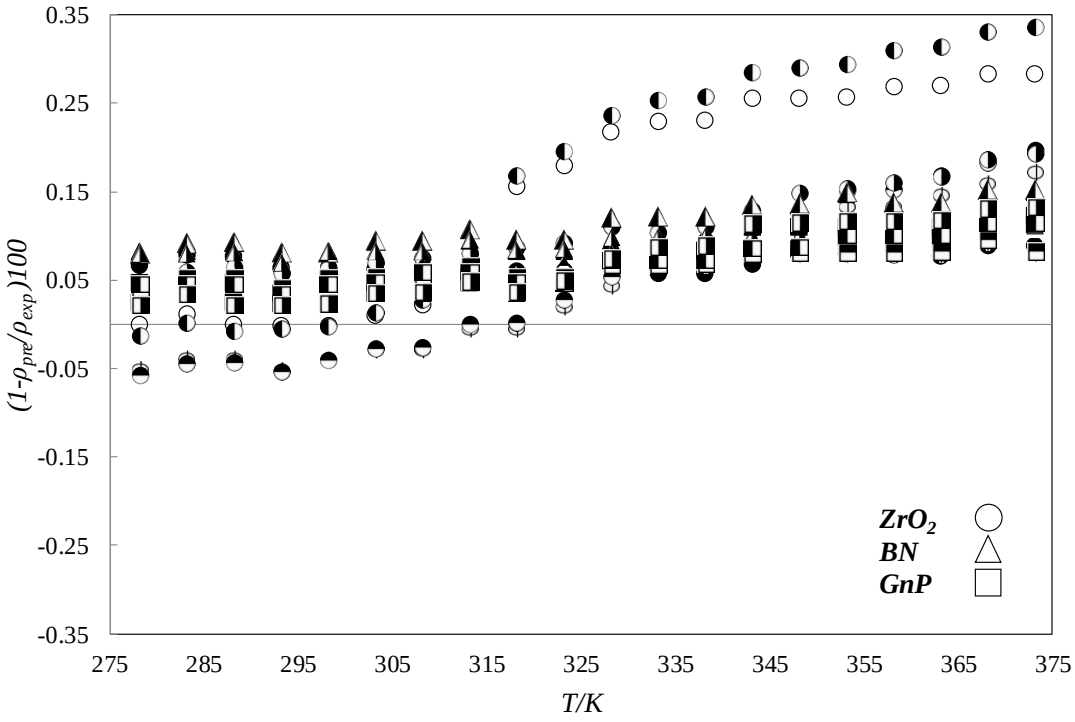

Fig. 17. Relative deviations between experimental density data (ρ_{exp}) and predicted values (ρ_{pre}). Pack and Cho [43]: (◫; ◬; ◫) 0.5 wt% ZrO_2 , 0.05 wt% BN and 0.05 wt% GnP; (○; △; □) 1 wt% ZrO_2 , 0.10 wt% BN and 0.10 wt% GnP; (●; ▲; ■) 2 wt% ZrO_2, 0.25 wt% BN and 0.25 wt% GnP. Wasp et al. [42]: (◓; ◬; ◓) 0.5 wt% ZrO_2 , 0.05 wt% BN and 0.05 wt% GnP; (◐; ◭; ◧) 1 wt% ZrO_2 , 0.10 wt% BN and 0.10 wt% GnP; (◑; ◭; ◨) 2 wt% ZrO_2, 0.25 wt% BN and 0.25 wt% GnP.

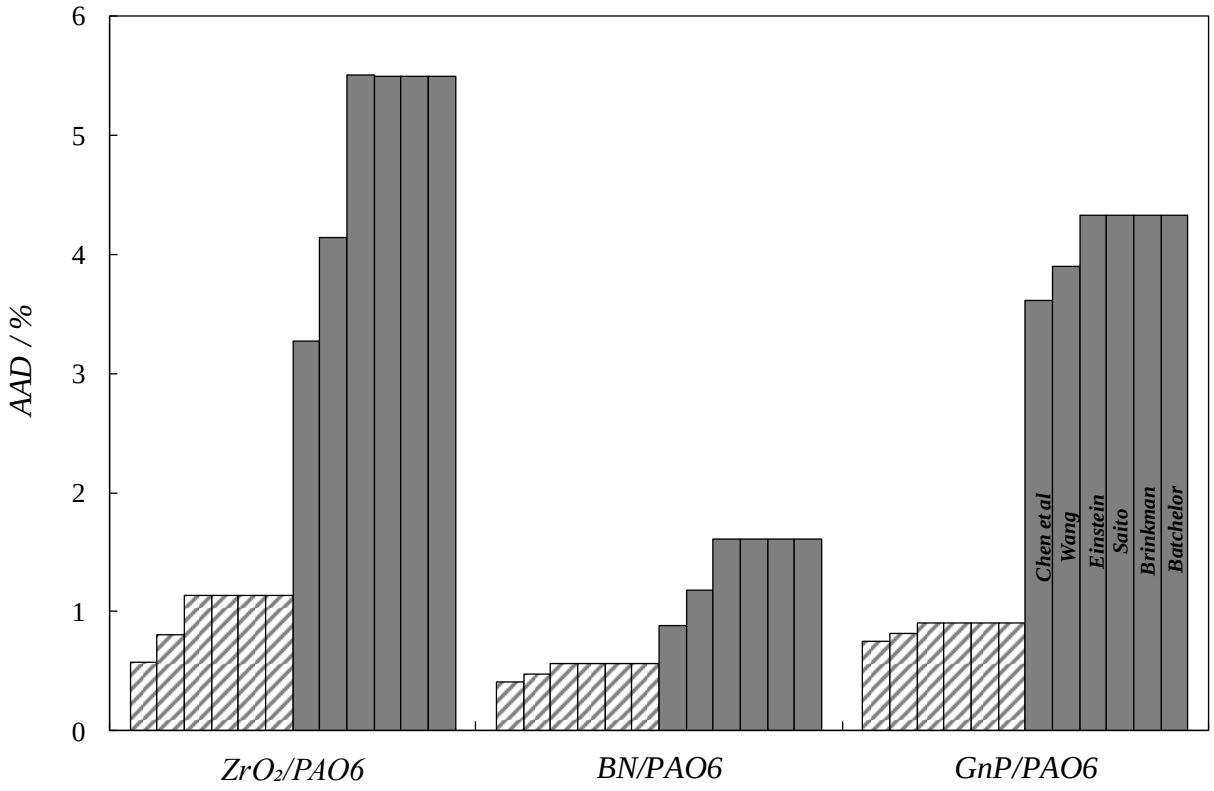

Fig. 18. Absolute average relative deviations (*AAD%*) between experimental viscosity data (η_{exp}) and predicted values (η_{pre}) by using viscosity models reported in Table 7: (▨) low concentration nanolubricants (0.5 wt% ZrO_2, 0.05 wt% BN and 0.05 wt% GnP) and (■) high concentration nanolubricants (2 wt% ZrO_2, 0.25 wt% BN and 0.25 wt% GnP).